NeuroImage 178 (2018) 435–444

Contents lists available at ScienceDirect

NeuroImage

journal homepage: www.elsevier.com/locate/neuroimage

Distinct neural circuits support incentivized inhibition

Josiah K. Leong [a], Kelly H. MacNiven [a,b], Gregory R. Samanez-Larkin [c], Brian Knutson [a,b,*]

[a] Department of Psychology, Stanford University, Stanford, CA, 94305-2025, USA
[b] Stanford Neuroscience Institute, Stanford University, Stanford, CA, 94305-2025, USA
[c] Department of Psychology and Neuroscience, Duke University, Durham, NC, 27708, USA

ARTICLE INFO

Keywords:
Reward
Response
Functional magnetic resonance imaging
Diffusion-weighted imaging
Ventrolateral prefrontal cortex
Anterior insula
Nucleus accumbens
Human
MIDI task

ABSTRACT

The ability to inhibit responses under high stakes, or "incentivized inhibition," is critical for adaptive impulse control. While previous research indicates that right ventrolateral prefrontal cortical (VLPFC) activity plays a key role in response inhibition, less research has addressed how incentives might influence this circuit. By combining a novel behavioral task, functional magnetic resonance imaging (FMRI), and diffusion-weighted imaging (DWI), we targeted and characterized specific neural circuits that support incentivized inhibition. Behaviorally, large incentives enhanced responses to obtain money, but also reduced response inhibition. Functionally, activity in both right VLPFC and right anterior insula (AIns) predicted successful inhibition for high incentives. Structurally, characterization of a novel white-matter tract connecting the right AIns and VLPFC revealed an association of tract coherence with incentivized inhibition performance. Finally, individual differences in right VLPFC activity statistically mediated the association of right AIns-VLPFC tract coherence with incentivized inhibition performance. These multimodal findings bridge brain structure, brain function, and behavior to clarify how individuals can inhibit impulses, even in the face of high stakes.

Introduction

People sometimes must rein in their impulses when stakes are high. Failure to do so not only can generate irrational or inconsistent behavior in the moment, but also can reduce the likelihood of survival and thriving over the long run. While different neural circuits may promote versus prohibit impulses, their distinct neural trajectories and interactions remain unclear (Mogenson et al., 1980; Graybiel, 1990; Robbins and Everitt, 1996; Ferenczi et al., 2016). Characterization of circuits that support incentivized inhibition might help identify neural targets relevant to the diagnosis and treatment of impulse control disorders.

Both lesion and neuroimaging research implicate the ventrolateral prefrontal cortex (VLPFC; often right lateralized) in inhibiting ongoing responses (Aron et al., 2003, 2007; Aron and Poldrack, 2006; Levy and Wagner, 2011), as well as in adjusting responses to changes in reward availability (Rudebeck et al., 2017). Meta-analyses of neuroimaging research on response inhibition, however, also associate right anterior insula (AIns) activity along with VLPFC activity in response inhibition (Swick et al., 2011; Cai et al., 2014). A different neuroimaging literature has implicated AIns and nucleus accumbens (NAcc) activity in the anticipation of incentives (Knutson and Greer, 2008). Distinctive contributions of response inhibition versus incentive anticipation circuits to incentivized inhibition, however, have yet to be characterized.

Comparative neuroanatomical findings could inform human neuroimaging research on incentivized inhibition (Jbabdi et al., 2015). Specifically, axon tracing studies of monkeys indicate that dense bidirectional monosynaptic projections connect the AIns to the VLPFC (Mufson and Mesulam, 1982; Mesulam and Mufson, 1982b; Lehman et al., 2011). More recently, researchers have used diffusion-weighted imaging (DWI) to visualize related tracts in humans (Cerliani et al., 2011; Cloutman et al., 2011). Beyond depicting tract trajectories, DWI measures such as fractional anisotropy (FA) and the inverse of mean diffusivity (MD) can index increased structural coherence in targeted tracts (Gomez et al., 2016). Structural coherence of an AIns-VLPFC tract, however, has yet to be assessed in humans or linked to brain activity and behavior. In contrast, unidirectional monosynaptic tracts projecting from the AIns to the NAcc (Chikama et al., 1997; Reynolds and Zahm, 2005) have recently been identified in humans (Leong et al., 2016), and may play a role in balancing avoidance against approach motivation, since their increased coherence appears to diminish the attractiveness of risky gambles by blunting NAcc activity (Leong et al., 2016).

While the impact of incentives on inhibition might critically inform

* Corresponding author. 450 Serra Mall, Building 420, Stanford, CA, 94305-2025, USA.
E-mail address: knutson@stanford.edu (B. Knutson).

https://doi.org/10.1016/j.neuroimage.2018.05.055
Received 8 December 2017; Received in revised form 12 May 2018; Accepted 23 May 2018
Available online 24 May 2018

studies of impulse control, researchers have only begun to explore the intersection of incentives and inhibition (Leotti and Wager, 2010; Padmala and Pessoa, 2010; O'Connor et al., 2012; Guitart-Masip et al., 2012; Dunovan et al., 2015). Current research has not yet independently varied incentive cues and inhibitory instructions on a trial-to-trial basis in order to control for potential confounds of expectation on behavior. Thus, a task that independently varies incentives and inhibition on each trial might clarify whether dissociable neural circuits can support processing incentives versus inhibition.

To characterize neural circuits that support incentivized inhibition, we first examined the effect of monetary incentives on response inhibition in a novel task that independently varied cued incentives and subsequent motor response requirements on a trial-to-trial basis (i.e., the Monetary Incentive Delay Inhibition or MIDI Task). Next, we examined whether functional brain activity in the right AIns and right VLPFC might improve, whereas activity in the NAcc might impair, incentivized inhibition performance (specifically under conditions involving high incentives as well as inhibition demands). We then identified and characterized structural white-matter tracts connecting the right AIns and VLPFC as well as the right AIns and NAcc, to test whether their coherence was associated with incentivized inhibition performance. Finally, we combined these multimodal neuroimaging measures and behavior in multivariate models to determine whether functional activity at key tract projection points could statistically account for observed associations of structural tract coherence with incentivized inhibition performance.

Materials and methods

Fifty-one right-handed adults recruited from the community completed the study. Eleven of these were excluded from analyses based on excessive head motion during the FMRI scan (i.e., greater than 2 mm in any plane between whole-brain acquisitions; n = 7; Wu et al., 2014), or DWI scan (i.e., greater than 5 mm in any plane on average across diffusion gradient directions; n = 4), leaving a remaining total of 40 subjects for analysis (18 females, age mean = 36, standard deviation = 14.3, range = 18–68 years). The study was conducted at the Stanford Center for Cognitive and Neurobiological Imaging. Written informed consent was obtained from all subjects prior to participation. After completing behavioral and self-report measures (including neuropsychological and personality tests), subjects then underwent functional and structural magnetic resonance scans (detailed below). Subjects received a fixed compensation of $20 per hour, as well as the total money that they earned on the task. The study was approved by the Stanford Medical School Institutional Review Board.

Experimental design and statistical analysis

The sample size of this study was motivated by robust effects of reward anticipation on mesolimbic brain activity in a well-established "Monetary Incentive Delay" (MID) task (Knutson et al., 2001; Knutson and Greer, 2008). Further, a power analysis based on a previously reported association between right AIns-NAcc tract coherence and behavioral preference for positively-skewed gambles indicated that a sample of at least 34 subjects should prove sufficient to observe predicted associations between the coherence of a single tract and behavior ($p < 0.05$, Cohen's d = 0.4, type I error = 0.05, power = 0.80, one-tailed test; G*Power 3.1; Leong et al., 2016). Moderate test-retest reliability of measures of anticipatory brain activity and of diffusion measures of VLPFC white matter have also been reported (Wu et al., 2014; Boekel et al., 2017). Overall, confirmatory analyses were tested at conventional thresholds (e.g., t-tests involving behavioral performance, regressions involving FMRI VOI activity; $p < 0.05$, bidirectional), while exploratory analyses were tested with more stringent thresholds using conventions commonly applied in the literature (e.g., whole-brain FMRI contrasts; described in the "FMRI acquisition and analysis" section). Bonferroni correction was applied where multiple tests were performed (e.g., regressions involving two different measures of tract coherence; described in the "Results" section). Potentially confounding accounts, however, were tested at the confirmatory thresholds in order to ensure direct comparability with the confirmatory tests. Code supporting the analyses is available on the Open Source Framework (http://doi.org/10.17605/OSF.IO/D3FKP; additional GitHub repositories with software versions are also described in the Materials and Methods). Relevant data are also available from the authors by request.

Behavioral task

Subjects underwent FMRI while performing a novel "Monetary Incentive Delay Inhibition" (MIDI) Task, during which they saw varying incentive cues and then responded to subsequently presented "go" or "no go" response targets (see Fig. 1). During each trial (N = 96; 12 per condition), subjects first saw an incentive cue (2 s) representing the amount of money they could gain or lose (+$5, +$0, –$5, –$0). Subjects then fixated on a centrally-presented cross during an anticipatory interval (2–2.5 s) while anticipating the appearance of an adaptively-timed target (<2 s), which indicated the motor response ("go" or "no go") required to obtain the incentive. Specifically, if the subject saw a go target (i.e., an upright solid triangle), they had to press a button as quickly as possible before the target disappeared. This go target was displayed for a variable interval, which temporally adapted with a staircase procedure to maintain subject performance on go trials for each incentive condition at approximately 66%. If the subjects instead saw a no go target (i.e., an inverted textured triangle), they had to withhold any motor response. No go target display times were not yoked to behavioral performance, and instead displayed for a variable interval (randomly generated between 500 and 750 ms). Next, subjects saw a monetary outcome based on their performance on that trial (2 s). Finally, subjects fixated on a centrally-presented cross (2–6 s) until the beginning of the next trial. Four different incentive conditions were presented with two motor response targets, for a total of eight trial conditions. The conditions thus constituted a full factorial design, such that each of the four

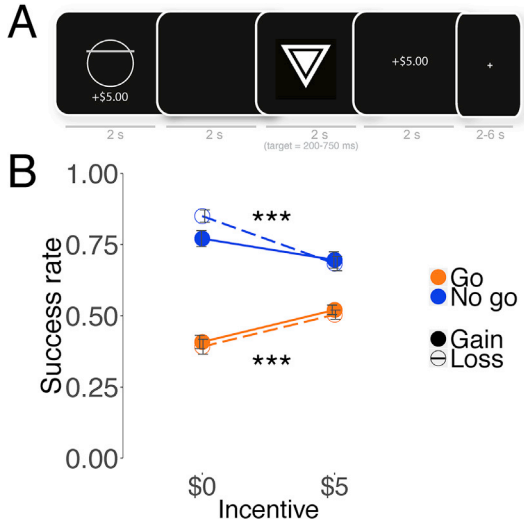

Fig. 1. Influence of incentive cues and inhibitory targets on behavior.
(A) Monetary Incentive Delay Inhibition (MIDI) Task trial structure. Subjects viewed a monetary incentive cue (2 s), anticipated responding (2 s), responded to a Go or No go target (variable timing), viewed the trial outcome (2 s), and fixated for a variable inter-trial interval (2–6 s)
(B) Incentive cues enhanced motor go responses (paired t (39) = 5.40, $p < 0.0001$), but impaired no go (inhibitory) responses (paired t (39) = −4.22, $p < 0.001$). Solid lines indicate gain cue trials, while dashed lines indicate loss cue trials; ***$p < 0.001$. See Table 1 for results from an omnibus analysis of variance test of behavioral performance.

incentive conditions was fully crossed with an equal number of go and no go motor targets. Subjects completed the MIDI task in two consecutive FMRI runs (each lasting 10 min) immediately subsequent to completing the Monetary Incentive Delay (or MID) task (Knutson et al., 2001). Subjects received a cumulative outcome based on their overall performance at the end of the experiment. Thus, if subjects lost money on the task, it was deducted from their hourly payment for research participation (average earnings = +$17.25, range = –$10.00 - +40.00, standard deviation = $13.91).

FMRI acquisition and analysis

Images were acquired in a 3 T Discovery MR750 scanner (GE Medical Systems, Milwaukee, WI) with a thirty-two channel head coil. Forty-six 2.9 mm thick slices (in-plane resolution 2.9 × 2.9 mm, interleaved acquisition) extended axially from the mid-pons to the top of the skull. Whole-brain functional scans were acquired with a T2*- weighted gradient pulse sequence (TR = 2 s, TE = 24 ms, flip angle = 77°, FOV = 232 mm, matrix size = 80 × 80). A T1-weighted anatomical scan was also collected using an axial fast spoiled grass sequence (0.9 mm isotropic voxels, TR = 7.2 ms, TE = 2.3 ms, flip angle = 12°) for co-registration of both functional images and diffusion-weighted images, as well as for volume of interest (VOI) specification.

Functional imaging analyses were conducted on functional scans indexing blood oxygen level dependent signal (hereafter referred to as "brain activity") using Analysis of Functional Neural Images (AFNI) software. For preprocessing, individual subject data were sinc interpolated to correct for non-simultaneous slice acquisition, corrected for motion in six dimensions, spatially smoothed using a small kernel (full width at half maximum = 4 mm), and high-pass filtered (omitting frequencies with period slower than 90 s). Visual inspection of motion correction estimates confirmed that seven subjects' heads had moved more than 2 mm in a plane from one whole-brain volume acquisition to the next, and so these were excluded from further analysis.

Whole-brain statistical analyses were performed with regression models that included regressors of no interest which included: (1) six regressors that indexed motion across volume acquisitions; (2) two regressors that indexed activity in cerebrospinal fluid and white matter volumes of non-interest; and (3) three that indexed the anticipation, target, and outcome periods across all trials. Ten orthogonal regressors of interest then contrasted: (1) gain versus non-gain anticipation; (2) loss versus non-loss anticipation; (3) go versus no go target; (4) hit versus miss motor response (irrespective of target type); (5) the interaction of gain versus non-gain cue and go versus no go target; (6) the interaction of loss versus non-loss cue and go versus no go target; (7) the interaction of gain versus non-gain anticipation, go versus no go target, and hit versus miss motor response; (8) the interaction of loss versus non-loss anticipation, go versus no go target, and hit versus miss motor response; (9) gain versus non-gain outcome; and (10) non-loss versus loss outcome. These mathematically orthogonal regressors of interest were convolved with a single gamma-variate function that modeled the canonical hemodynamic response (Cohen, 1997) before inclusion in the regression model. Collinearity analysis of the design matrix confirmed the statistical independence of the regressors of interest (see Supplementary Fig. 1). For group statistical maps, individual subjects' t-statistic maps of regressors of interest were transformed to Z-scores, spatially warped to Talairach space, and resampled into 2 mm cubic voxels. Group maps were voxel-wise thresholded ($p < 0.001$), and then cluster thresholded (cluster size > 5 contiguous 2.9 mm cubic voxels) to yield corrected maps for detecting activity within a gray matter mask ($p < 0.05$ corrected, derived with 10,000 Monte Carlo iterations using the program 3dClustSim in AFNI version AFNI_18.0.25, which automatically estimates spatial autocorrelation to minimize false positive findings).

To extract raw activity time courses for targeted analyses, spherical volumes of interest (VOIs; 8 mm diameter) were centered on bilateral foci for the NAcc (Talairach coordinates: ±10, 12, −2), AIns (±34, 24, −4), and MPFC (±4, 45, 0), based on coordinates specified in previous research on incentive processing (Knutson and Greer, 2008). Additional VOIs were centered on bilateral foci for VLPFC (±45, 30, 0) and DLPFC (±31, 15, 44) activity, based on the whole-brain group contrast maps. The coordinates for the VLPFC VOI were based on the whole-brain contrast of neural responses to go versus no go targets, rather than subjects' motor responses. VOIs were warped from Talairach space to subjects' native brain space, and activity was spatially averaged within each VOI and then divided by the mean activity over the entire experiment to derive a continuous measure of percent signal change. Confirmatory analyses were performed using VOIs from the Desai probabilistic atlas, to best match the subject-specific FreeSurfer VOIs used for tractography analyses. Time courses were then shifted two volume acquisitions (or 4 s) to account for the hemodynamic response lag to peak response. Percent signal change was extracted from trial periods when subjects viewed incentive cues (i.e., the first volume acquisition), anticipated responding for those incentives (second volume acquisition), and responded to the go or no go target in each trial (third volume acquisition). Specifically, activity was extracted from the NAcc and AIns when subjects viewed incentive cues, from the MPFC when subjects anticipated responding for those incentives, and from the VLPFC and DLPFC when subjects responded to targets. The timing of relevant brain activity was based on the componential and hierarchical Affect-Integration-Motivation framework, which predicts that neural affective responses can precede and modify subsequent value integration, which then informs motivated responses (Samanez-Larkin and Knutson, 2015). These were included in logistic regression models that used brain activity to predict trial-to-trial behavioral performance (success or failure in responding appropriately to the go or no go target), with subjects modeled as random effects. Brain activity in any VOI that was greater than 3 standard deviations from the mean percent signal change in that VOI was excluded from regression models. Statistical analyses were performed in R (version 3.4.0), using packages for mixed effects regression analysis (lme4 version 1.1–15), statistical mediation analysis (lavaan version 0.5–23.1097), and data visualization (ggplot2 version 2.1.1). Whole brain FMRI contrast maps are available on NeuroVault (https://neurovault.org/).

Diffusion-weighted MRI acquisition

Diffusion-weighted images were acquired on the same 3 T Discovery Magnetic Resonance 750 scanner (GE Medical Systems, Milwaukee, WI). A diffusion-weighted, dual spin-echo, echo-planar imaging sequence (TR = 9600 ms, TE = 97.5 ms, flip angle = 90°, FOV = 240 mm, matrix size = 120 × 120) was used to acquire sixty 2 mm-thick slices in 96 different diffusion directions (b = 2500). Ten non-diffusion-weighted (b = 0) volumes were acquired.

Diffusion-weighted MRI preprocessing

Anatomical landmarks were manually defined in the anterior and posterior commissures (AC-PC), and the midsagittal plane to guide a rigid-body transformation that converted the T1-weighted structural images into AC-PC aligned space. Each diffusion-weighted image was then registered to the mean of the motion-corrected non-diffusion-weighted (b = 0) images. The mean of the non-diffusion-weighted images was aligned to the T1-weighted image in AC-PC space using a rigid body transformation. Finally, all raw diffusion images were aligned to AC-PC space by combining motion correction, eddy-current correction, and anatomical alignment into a single transformation, and then resampled to 2 mm isotropic voxels. All preprocessing steps were performed using the open-source mrDiffusion package (www.github.com/vistalab/vistasoft) in MATLAB R2013a (version 8.1.0.604).

Volume of interest (VOI) identification

To define anatomical VOIs to seed for tractography analyses, each

subject's AC-PC aligned T1-weighted image was processed through FreeSurfer, an automatic segmentation and parcellation software suite (version 5.3.0; Fischl et al., 2004). NAcc VOIs were identified from probabilistic classification of subcortical tissue based on a manually-labeled training set (Desikan et al., 2006). AIns VOIs for the AIns-NAcc tract were derived from the Destrieux cortical parcellation atlas, by combining the anterior insula and short gyrus parcellations (Destrieux et al., 2010; Leong et al., 2016). For the AIns-VLPFC tract, only the short gyrus parcellation was included in the AIns VOI, since the Destrieux cortical parcellation of the anterior insula includes part of the frontal operculum. Thus, tracing tracts between the VLPFC and the Destrieux cortical parcellation of the anterior insula would erroneously include fibers that remain in the inferior frontal gyrus, rather than combining with the uncinate fasciculus before diverging to terminate in the anterior insula (contrary to tract trajectories described in anatomical studies of monkeys; Lehman et al., 2011). VLPFC VOIs were derived from the frontal-orbital parcellation of the Destrieux atlas. The VLPFC VOI is consistent with the region used in anatomical studies of monkeys (also identified as Brodmann area 47; Mufson and Mesulam, 1982; Mesulam and Mufson, 1982b; Petrides and Pandya, 2001). A binary mask was formed using the gray versus white-matter border identified by FreeSurfer to restrict fibers to brain white matter.

Control tracts were also traced to verify the specificity of predicted associations between brain structure, brain activity, and behavior. These control tracts were selected based on their previously-documented associations with response inhibition. Specifically, the VLPFC-STN tract has been called the "hyperdirect pathway" based on its role in stopping ongoing action (as in the Stop Signal Task; Aron et al., 2003). The preSMA-STN tract has also been implicated in response inhibition (Rae et al., 2015). The MPFC-NAcc tract was selected based on its role in guiding incentivized choices and altering NAcc brain activity (Samanez-Larkin et al., 2012; Ferenczi et al., 2016). PreSMA VOIs were defined by obtaining the superior frontal gyrus parcellation from FreeSurfer, and longitudinally masking it from the anterior commissure to the genu of the corpus callosum (Johansen-Berg et al., 2004). STN VOIs were defined by taking the ventral diencephalon segmentation from FreeSurfer, and masking a $10 \times 10 \times 10$ mm box centered around Talairach coordinates ($\pm 10, -15, -5$), following previously-described methods (Aron et al., 2007). MPFC VOIs (8 mm diameter) were manually placed as described in previous research (Samanez-Larkin et al., 2012).

Probabilistic tractography

Fiber tracking between VOIs (AIns-NAcc, Ains-VLPFC, VLPFC-STN, and preSMA-STN) was performed using constrained spherical deconvolution-based probabilistic tracking, as implemented in the Mrtrix software (version 0.2.12; Tournier et al., 2007). The maximum number of harmonics was set to ten ($L_{max} = 10$), which defined the maximum number of deconvolution kernels utilized by constrained spherical deconvolution to estimate the fiber orientation distribution function in each voxel. Fiber pathways were generated by randomly seeding a voxel in a starting VOI and tracking until the fiber reached the ending VOI (number = 5,000,000, maxnum = 5000). Start and end VOIs were seeded randomly to ensure symmetrical fiber tracking. Fibers leaving the white-matter volume were terminated and discarded. The MPFC-NAcc tract was traced using previously-described methods (Sherbondy et al., 2008; Samanez-Larkin et al., 2012; Leong et al., 2016).

Fibers obtained from the tractography solutions were then reduced to core fiber bundles by eliminating outliers and anatomically unlikely pathways (e.g., fibers crossing the cerebral hemispheres, or crossing through cerebrospinal fluid). Specifically, fibers longer than 2 standard deviations from the mean fiber length were initially removed. Next, fibers greater than 3 standard deviations away from the mean spatial position of the core fiber (Mahalanobis distance) were removed. Finally, fibers that took indirect routes between VOIs were removed (e.g., those that projected in one direction but then looped backward).

Diffusion measure calculation

After identifying each tract, we quantified measures of their structural coherence. Specifically, diffusion properties of each fiber bundle can be characterized by obtaining mean fractional anisotropy (FA) and mean diffusivity (MD) for each identified tract (Basser and Pierpaoli, 1996). Both FA and MD can vary as a function of fascicle density, axon diameter, and myelination (Jones et al., 2013; Chang et al., 2017), but while greater FA typically indexes increased tract coherence, greater MD instead indexes decreased tract coherence. To assess variation in diffusion properties along each tract's trajectory, we spatially normalized fiber pathways between subjects by sampling 100 evenly-spaced cross-sectional nodes along the fiber length of each tract from the starting VOI to the ending VOI (Yeatman et al., 2012). The mean diffusion metric in each node was then calculated as an average of each fiber's metric in that node, weighted by the spatial distance of that fiber from the node's core fiber. We then averaged each metric across the middle 50% of nodes along each pathway to ensure that coherence measures exclusively included white matter but not voxels along the gray versus white-matter boundary. Indexing tract coherence in the middle half of each tract follows previous tractography methods, and can minimize the influence of branching axons at the end of cortical tracts (Yeatman et al., 2012). This procedure generated single FA and MD values for each tract in each hemisphere of every subject. Since greater FA and lesser MD independently index distinct aspects of increased tract coherence, we inverted MD values (1 minus MD) to facilitate interpretation of findings. The instructions and open-source code for assessing these qualities for each tract are available on GitHub (https://github.com/josiahl/spantracts).

Results

Incentive cues improve go performance, but impair no go performance

Subjects performed better at "go" motor responses for large incentives than for no incentives (+/−$5 versus +/−$0, paired $t(39) = 5.40$, $p < 0.0001$; see Fig. 1), but worse at "no go" motor responses for large incentives than for no incentives (+/−$5 versus +/−$0, paired $t(39) = -4.22$, $p < 0.001$). This behavioral dissociation reliably persisted across both halves of the task (see Supplementary Fig. 2). Subjects also performed better at "no go" motor responses to avoid a non-incentivized loss than a non-incentivized gain (–$0 versus +$0, paired $t(39) = 3.87$, $p < 0.001$). An omnibus repeated-measures analysis of variance confirmed the predicted interaction of incentives and inhibition, such that both gain and loss incentives decreased inhibition performance (see Table 1).

Accordingly, incentives sped reaction times for both successful go responses and failed no go responses (paired $t(30) = -2.06$, $p = 0.048$; see also Supplementary Fig. 2). A signal detection analysis revealed that while incentives did not change the sensitivity to respond to targets (d-prime), incentives did reduce (or liberalize) the criterion (c) for responding to targets, or the threshold for making a response (see Supplementary Fig. 3). Since the criterion was associated with earnings ($r = 0.37$, $p = 0.02$), these findings suggested that incentives paradoxically induced suboptimal performance in most subjects.

Temporal stability analyses revealed low split-half reliability for go performance, but moderate split-half reliability for no go performance (Go: ICC2k = −0.14, $p = 0.67$; No go: ICC2k = 0.60, $p < 0.0001$). No go performance was particularly reliable in high gain trials (+$5: ICC2k = 0.56, $p = 0.002$; –$5: ICC2k = 0.15, $p = 0.28$; +$0: ICC2k = 0.55, $p = 0.001$; –$0: ICC2k = 0.48, $p = 0.02$; in which ICC2k represents the intraclass correlation coefficient for the average measure of a randomly-selected individual). Since the condition of interest showed high reliability, we focused our analyses on incentivized inhibition (or +$5 no go) trials to examine whether brain structure and function could account for individual differences in performance (see Supplementary Table 1 as well as Supplementary Table 2 for analyses

Table 1
Behavioral performance in the MIDI Task.

Contrast	Coefficient	Standard error	t-value	p-value
Gain > loss	−0.001	0.009	−0.150	0.881
$5 > $0	0.003	0.009	0.389	0.697
No go > go	0.146	0.009	16.794	<0.001
Gain $5/loss $0 > loss $5/gain $0	0.011	0.009	1.227	0.221
Gain no go/loss go > gain go/loss no go	−0.015	0.009	−1.766	0.078
$5 no go/$0 go > $5 go/$0 no go	−0.058	0.009	−6.616	<0.001
Gain $5 no go/gain $0 go/loss $5 go/loss $0 no go > Gain $5 go/gain $0 no go/loss $5 no go/loss $0 go	0.013	0.009	1.527	0.128

A two (incentive cue valence: gain versus loss) by two (incentive cue magnitude: $5 versus $0) by two (target response requirement: "go" versus "no go") repeated measures analysis of variance was conducted on behavioral performance during the MIDI Task. Planned contrasts for incentives compared gain versus loss conditions (+1 versus −1) and $5 versus $0 conditions (+1 versus −1). The contrast for motor response was set as −1 for "go" versus +1 for "no go". The full model significantly accounted for behavioral performance (adjusted $R^2 = 0.51$, $F(7,312) = 47.56$, $p < 0.001$). Predicted contrasts indicated that subjects performed better overall in response to no go targets than in response to go targets ($t = 16.79$, $p < 0.001$). Incentive cues and motor response targets interacted, such that both gain and loss incentives decreased "no go" performance ($t = -6.62$, $p < 0.001$).

that depict these associations across all conditions).

Right AIns and VLPFC activity promotes but NAcc activity prohibits incentivized inhibition performance

To verify brain activity associated with incentive cue and inhibition target manipulations, we contrasted whole brain activity (1) when individuals anticipated gains of +$5 versus +$0 during cue presentation; (2) when individuals were presented with a go versus no go target during target presentation; and (3) the interaction of gain versus non-gain anticipation and go versus no go targets during target presentation. Whole brain statistical maps revealed robust activity in mesolimbic dopamine projection targets when individuals anticipated a +$5 versus +$0 gain (see Fig. 2). In contrast, right VLPFC showed increased activity in response to presentation of no go versus go targets. Finally, the interaction of these effects robustly activated bilateral dorsolateral prefrontal cortex (DLPFC), such that activity was greatest for trials in which +$5 cues preceded no go targets (see Fig. 2 and Supplementary Table 3).

Subjects participated in the MIDI task immediately after completing a Monetary Incentive Delay (or MID) task that lacked the response inhibition requirement of the MIDI task (Knutson et al., 2001). This allowed us to directly compare whether brain activity associated with anticipation of incentives might decrease in the context of response inhibition demands, and also to test whether behavioral performance and brain activity in the MID task could account for findings in the MIDI task. Analyses indicated that while anticipatory activity did not diminish in the MIDI versus the MID task, behavioral performance and brain activity during the MID task could not account for incentivized inhibition performance during the subsequent MIDI task (see Supplementary Fig. 5).

We next examined whether brain activity during incentive anticipation could predict subsequent behavioral responses to inhibition targets within subjects on a trial-to-trial basis. To do so, we extracted peak-lagged FMRI activity from predefined volumes of interest (VOIs) during the incentive cue and anticipation periods of each trial (see Materials and Methods). AIns and NAcc activity during incentive cue presentation were entered into logistic regressions that predicted trial-to-trial successful response inhibition for +$5. As predicted, increased right AIns activity in response to +$5 cues predicted successful inhibition of responses to no go targets, but increased right NAcc activity in response to +$5 cues instead predicted failure to inhibit responses to no go targets (see Table 2). Increased right MPFC activity during anticipation also predicted successful response inhibition to no go targets across all incentive conditions. Models that included left hemisphere VOI activity did not improve model fit, and addition of left hemisphere VOI terms did not reduce the right hemisphere effects, suggesting sufficiency of models containing only right hemisphere activity (see Supplementary Table 4). Models that included activity from caudate and anterior cingulate control VOIs also did not diminish the observed effects (see Supplementary Table 4). A confirmatory analysis substituting alternative VOI specifications yielded similar results (i.e, with VOIs derived from the Desai probabilistic atlas which better approximated subject-specific VOIs used in tractography analyses; see Supplementary Table 4). Right AIns and NAcc VOI activity did not predict performance in other incentive cue or motor target conditions, unlike MPFC activity, which predicted increased response inhibition across all conditions (see Supplementary Table 5).

Right VLPFC activity alone in response to targets did not predict incentivized inhibition performance on a trial-to-trial basis (see Table 2). Right VLPFC activity did predict successful response inhibition on a trial-to-trial basis, however, after including activity from control VOIs (see Supplementary Table 4). Further, individual differences in average right VLPFC activity in response to no go targets were also associated with better incentivized inhibition performance ($\beta = 0.42$, $t(38) = 2.84$, $p = 0.007$). The central coordinates of this VLPFC VOI (Talairach: 45, 30, 0) were also labeled in the Tourneaux-Talairach atlas as Brodmann area 47, consistent with individually seeded VOIs in the diffusion tractography analyses presented below, as well as tracings of connections between the AIns and VLPFC in previous anatomical studies of monkeys (Mufson and Mesulam, 1982; Mesulam and Mufson, 1982b; Petrides and Pandya, 2001). While this localization of VLPFC activity is consistent with anatomical studies, its coordinates are ventral to those described in other neuroimaging studies using inhibitory tasks (such as the stop-signal task; Aron and Poldrack, 2006; Aron et al., 2007). We next examined whether white-matter tracts connecting the AIns and VLPFC and AIns and NAcc could be identified, and tested whether measures of their coherence might be associated with incentivized inhibition performance.

Structural right AIns-VLPFC and AIns-NAcc tract coherence is associated with incentivized inhibition performance

We performed probabilistic tractography on DWI data to identify novel white-matter tracts connecting the AIns and the VLPFC, as well as the AIns and the NAcc (see Fig. 3). Next, we statistically validated evidence for each tract's existence using a virtual lesion method (see Supplementary Fig. 6; Pestilli et al., 2014). Next, to quantify each tract's coherence, we extracted fractional anisotropy (FA) and mean diffusivity (MD) measures based on a standard tensor model (Basser and Pierpaoli, 1996). Since greater FA and lesser MD can independently index aspects of increased tract coherence, we inverted MD values (1 minus MD) to facilitate interpretation of the results. FA and MD profiles were plotted along the trajectory of each tract in each hemisphere in every subject, and then averaged across the middle 50% portion of each tract's profile to generate indices of tract coherence (see Materials and Methods).

Coherence of the right AIns-VLPFC tract (inverse MD) was associated with incentivized inhibition performance when both tract coherence measures (FA and inverse MD) were included in the regression model (AIns-VLPFC FA: $\beta = -0.04$, $t(37) = -0.23$, $p = 0.82$; AIns-VLPFC inverse MD: $\beta = 0.39$, $t(37) = 2.58$, $p = 0.01$; all coefficient estimates are standardized). Coherence of the AIns-NAcc tract (FA) was also associated with incentivized inhibition performance in a similar model (AIns-NAcc FA: $\beta = 0.33$, $t(37) = 2.23$, $p = 0.03$; AIns-NAcc inverse MD: $\beta = 0.28$, $t(37) = 1.91$, $p = 0.06$). Pairwise correlations specifically revealed that coherence of the right AIns-VLPFC tract was associated with increased inhibition for high gains (AIns-VLPFC inverse MD: $\beta = 0.39$, $t(38) = 2.62$, $p = 0.01$); and that coherence of the right AIns-NAcc tract

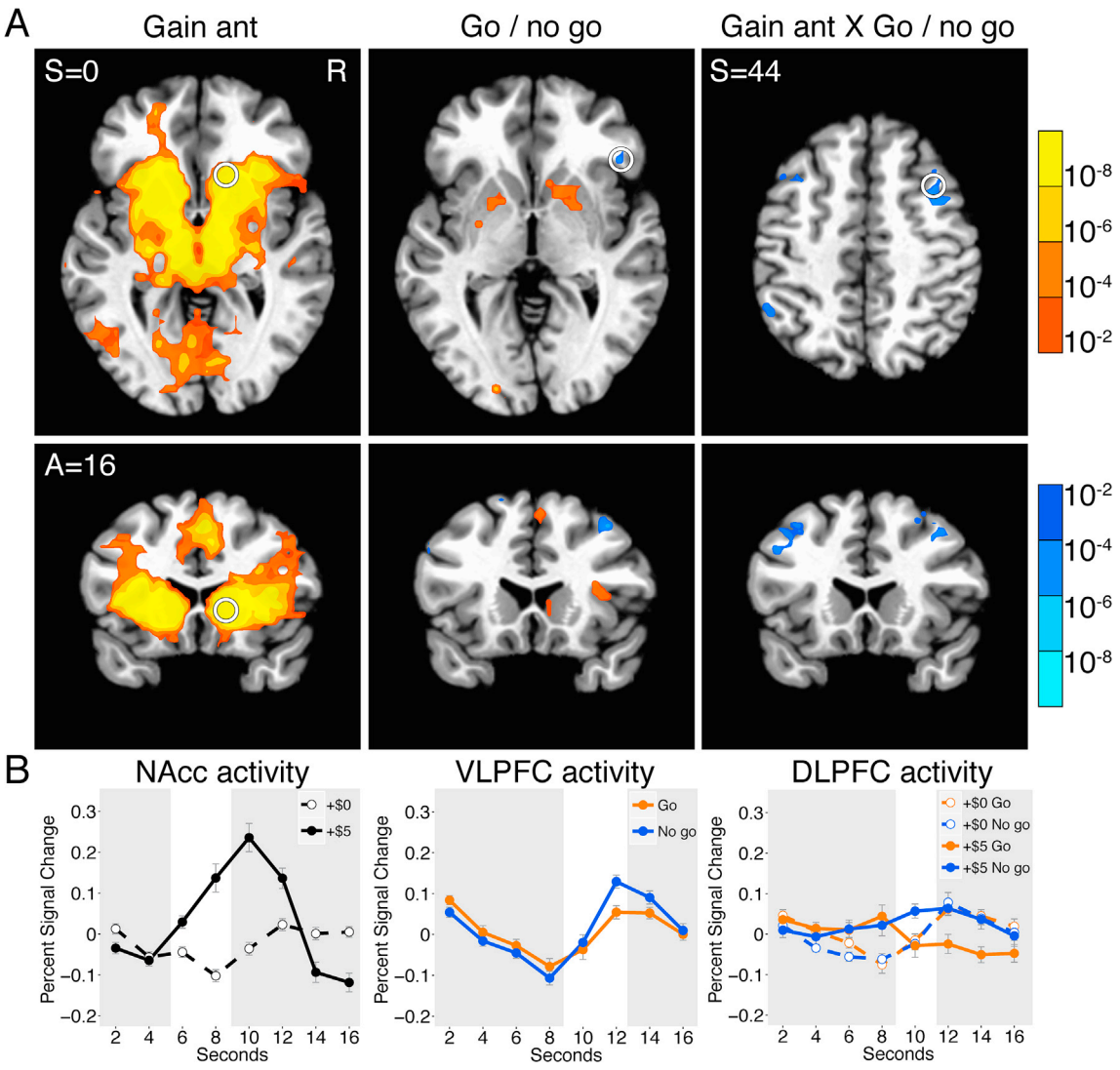

Fig. 2. Brain activity associated with incentive cues and inhibitory targets in the Monetary Incentive Delay Inhibition (MIDI) task. (**A**) Contrast maps depict main effects of anticipating gains versus non-gains (Gain ant), go versus no go target presentation (Go/no go), and their interaction (Gain ant X Go/no go) on brain activity. Warm colors indicate increased activity while cool colors indicate decreased activity for relevant contrasts (S = superior; A = anterior; R = right). Maps were thresholded voxelwise $p < 0.001$, and cluster corrected $p < 0.05$ (see Materials and Methods; see also Supplementary Fig. 4 for equivalent contrast maps for monetary loss conditions). (**B**) Averaged activity time courses extracted from volumes of interest show greater right NAcc activity during anticipation of gain versus non-gain, greater right VLPFC activity in response to no go versus go targets, and greater right DLPFC activity in response to no go targets following gain anticipation. White bars highlight trial phases predicted to show differential activity. NAcc activity did not differ prior to presentation of go versus no go targets, suggesting that it did not reflect differential motor preparation (see Supplementary Fig. 4; see also Supplementary Fig. 5 for comparison of NAcc activity in the Monetary Incentive Delay task without an inhibition component; Knutson et al., 2001).

was also associated with increased inhibition for high gains (AIns-NAcc FA: $\beta = 0.37$, $t(38) = 2.48$, $p = 0.02$). Both of these associations survived correction for testing associations between two indices of tract coherence (i.e., FA and inverse MD) and behavior (corrected threshold $p = 0.025$). Measures of coherence of both tracts remained significantly associated with incentivized inhibition performance after including them the same model, suggesting that these measures indexed distinct aspects of incentivized inhibition (AIns-VLPFC inverse MD: $\beta = 0.36$, $t(37) = 2.51$, $p = 0.02$; AIns-NAcc FA: $\beta = 0.34$, $t(37) = 2.38$, $p = 0.02$). Bootstrapped correlations ($n = 10{,}000$) confirmed the robustness of both the association between right AIns-VLPFC tract coherence and incentivized inhibition performance (95% confidence interval: 0.40, 7.02), and the association between AIns-NAcc tract coherence and incentivized inhibition performance (95% confidence interval: 0.22, 2.66). Controlling for age and coherence of left hemisphere tracts did not diminish these effects (see Supplementary Table 6, and Materials and Methods). Controlling for coherence metrics of control tracts also did not diminish these effects (see Supplementary Fig. 6 and Supplementary Table 6). Further, AIns-VLPFC and AIns-NAcc tract coherence metrics were not associated with behavioral performance in any other condition (see Supplementary Table 1 for full regression results).

Functional brain activity mediates the association of structural tract coherence with incentivized inhibition behavior

Individual differences in right VLPFC activity could statistically account for the association of right AIns-VLPFC tract coherence with incentivized inhibition performance (see Fig. 4). Results from a bootstrapped path analysis model (number of bootstraps = 10,000) indicated that right AIns-VLPFC tract coherence was associated with greater right VLPFC activity during +$5 cue no go responses ($\beta = 0.42$, $p = 0.009$), and that greater right VLPFC activity was associated with successful

Table 2
Brain activity predicts trial-to-trial incentivized inhibition performance.

Variable	Function only	Structure and function	Structure × function interaction
Previous trial go success	0.99 (0.25, 0.25)	0.96 (0.24, 0.25)	1.10 (0.28, 0.25)
Previous trial no go success	−0.19 (−0.06, 0.29)	−0.24 (−0.07, 0.29)	−0.25 (−0.07, 0.30)
R NAcc cue	−2.01* (−0.65, 0.33)	−1.90 (−0.62, 0.35)	−2.71** (−4.66, 1.72)
R AIns cue	2.55* (0.82, 0.33)	2.47* (0.78, 0.32)	−0.97 (−1.69, 1.75)
R MPFC anticipation	3.92*** (0.83, 0.21)	3.94*** (0.83, 0.21)	3.80*** (0.81, 0.21)
R VLPFC target	0.67 (0.15, 0.22)	0.64 (0.14, 0.22)	0.72 (0.16, 0.23)
R DLPFC target	−0.61 (−0.23, 0.38)	−0.84 (−0.32, 0.38)	−0.83 (−0.33, 0.39)
R AIns-NAcc FA		2.36* (6.98, 2.96)	2.43* (7.70, 3.17)
R NAcc*AIns-NAcc FA			2.39* (18.08, 7.56)
R AIns*AIns-NAcc FA			1.44 (11.49, 7.96)
Pseudo R^2	0.16	0.17	0.23
AIC	557	554	545
LOOCV %	71.5%	69.6%	71.9%

Z-scores with coefficient estimates and SE in parentheses. ***p < 0.001, **p < 0.01,*p < 0.05.

Logistic regression models (which included subjects as random effects) used brain VOI activity during incentive cue, anticipation, and target presentation trial phases to predict successful inhibition in response to high gain cues (+$5) on a trial-to-trial basis. Models controlled for response success in the previous trial (successful go or successful no go). The model including brain structure improved model fit, based on pseudo R^2, AIC, and a likelihood-ratio test of nested models (χ^2 (2) = 12.44, p = 0.002). Leave-one-subject-out cross validation verified that the models could predict trial-to-trial behavior in held-out subjects, and indicated that including an interaction term of brain structure and brain function did not induce overfitting. Models including left hemisphere tract coherence and VOI activity did not improve model fit, supporting the sufficiency of the right hemisphere-only model (see Supplementary Table 4). Inclusion of activity from control VOIs (i.e., in the caudate and anterior cingulate) also could not account for the observed effects (see Supplementary Table 4).

incentivized inhibition performance (β = 0.31, p = 0.04). Including the indirect effect of right VLPFC activity reduced the direct association of right AIns-VLPFC tract coherence with successful incentivized inhibition performance to non-significance (β = 0.26, p = 0.17), consistent with statistical mediation. Bootstrapped estimates of the indirect effect (number of bootstraps = 10,000) indicated a significant effect from structural tract coherence to functional activity to incentivized inhibition behavior (95% confidence interval: 0.04, 0.29). An alternative mediation model in which incentivized inhibition behavior instead mediated the effect of structural tract coherence on functional activity achieved the same model fit as the original model, but the indirect effect in this model was not statistically significant (95% confidence interval: −0.24, 0.02; see Supplementary Table 7). While this alternative model did not statistically differ from the original model overall, the original model better captured our causal prediction that brain structure should influence brain function, which should then influence behavior. No other combination of brain structure and function showed a similarly significant pattern of associations (see Supplementary Table 7).

To verify that right AIns-VLPFC tract coherence was associated with increased right VLPFC activity specifically during incentivized inhibition trials, we conducted a repeated-measures multivariate analysis of variance. Results revealed that right AIns-VLPFC tract coherence was associated with right VLPFC activity across all task conditions (F (1,38) = 6.91, p = 0.01), but also that right VLPFC activity differed across task conditions (F (7,266) = 2.36, p = 0.02). This analysis did not reveal a significant interaction, however, between right AIns-VLPFC tract

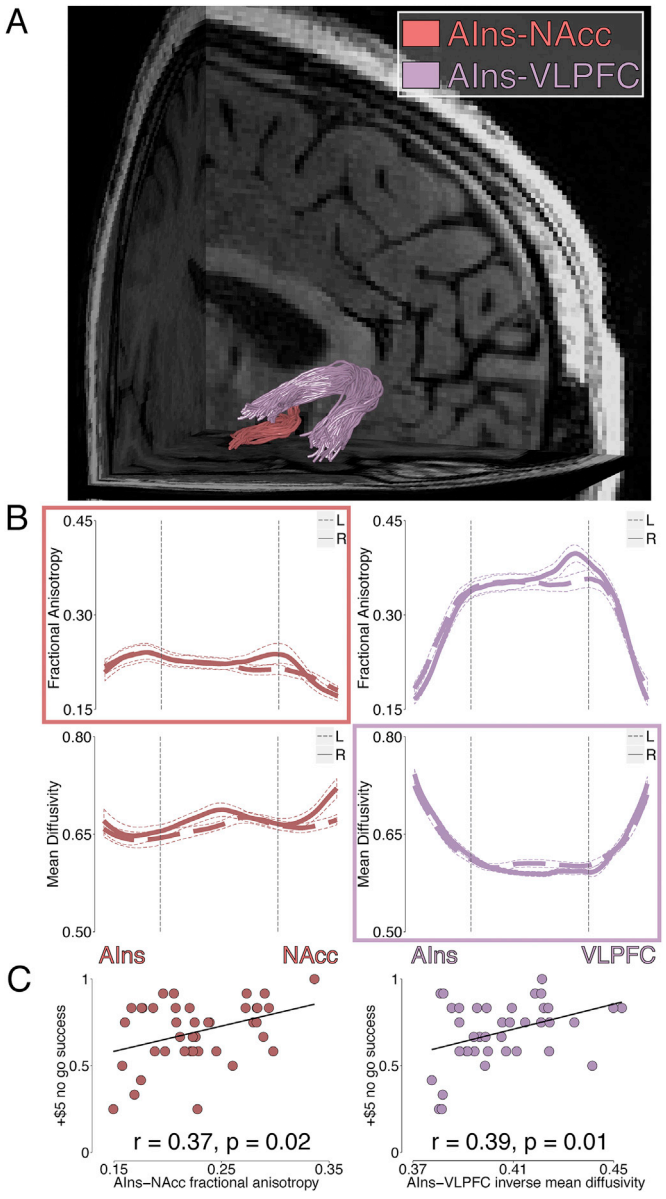

Fig. 3. Characterization of white-matter tracts and associations with behavior. (**A**) Right hemisphere tracts for a representative subject. The AIns-VLPFC tract exits the extreme capsule and travels with the uncinate fasciculus before entering the inferior frontal gyrus. The AIns-NAcc tract travels along the lateral-medial axis within the subcaudate white matter (see Supplementary Fig. 7 for additional tract visualizations; Leong et al., 2016). (**B**) Tract coherence profiles for the bilateral AIns-NAcc and AIns-VLPFC tracts. Fractional anisotropy (FA) and mean diffusivity (MD) are plotted at 100 cross sections from tract beginning to end. Mean values across subjects are displayed with standard errors (solid lines indicate the right hemisphere tract while dashed lines indicate the left). Mean FA and mean MD were obtained for each subject by averaging across the middle 50% of the tract in each hemisphere. Greater FA indicates increased tract coherence, but lesser MD indicates increased tract coherence. Measures of coherence in both tracts exhibited high test-retest reliability in a separate sample (see Supplemental Fig. 7). (**C**) Associations of tract coherence metrics with incentivized inhibition performance. Greater coherence of both the right AIns-VLPFC tract (inverse MD) and AIns-NAcc tract (FA) were associated with increased incentivized inhibition performance (AIns-VLPFC inverse MD: β = 0.39, t (38) = 2.62, p = 0.01; AIns-NAcc FA: (β = 0.37, t (38) = 2.48, p = 0.02). Controlling for coherence of control tracts did not alter observed associations of tract coherence with behavior (see Supplementary Fig. 6 and Supplementary Table 6).

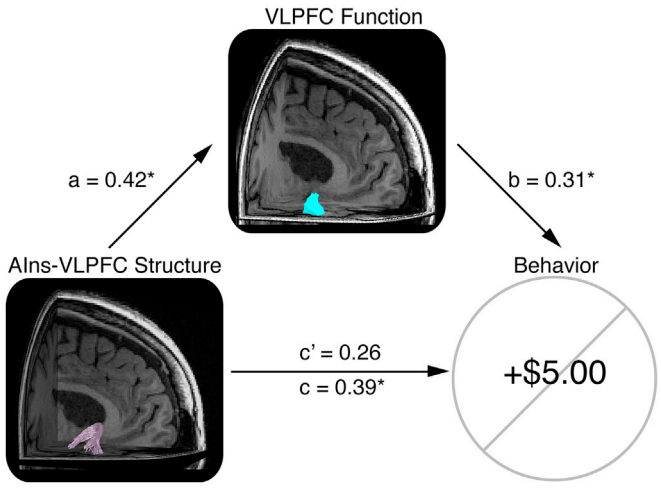

Fig. 4. Right VLPFC activity mediates the association of AIns-VLPFC structure with incentivized inhibition behavior. A mediation model tested whether AIns-VLPFC tract coherence could facilitate successful incentivized inhibition performance by promoting VLPFC activity. Right AIns-VLPFC tract coherence was associated with greater right VLPFC activity during +$5 cue no go responses ($\beta = 0.42$, $p = 0.01$), and greater right VLPFC activity was associated with increased incentivized inhibition performance ($\beta = 0.31$, $p = 0.04$). Including the indirect effect of VLPFC activity decreased the direct association of AIns-VLPFC tract coherence with incentivized inhibition performance to non-significance ($\beta = 0.26$, $p = 0.17$), consistent with statistical mediation. Control combinations of brain structure and function did not yield the same pattern of associations (see Supplementary Table 7).

coherence and experimental condition on right VLPFC activity ($F(7,266) = 1.59$, $p = 0.14$), suggesting that right AIns-VLPFC tract coherence was associated with right VLPFC activity across task conditions, although this activity may have been higher in the incentive conditions ($5 versus $0 right VLPFC activity: paired $t(39) = 2.37$, $p = 0.02$; see Supplementary Table 2).

As with AIns-VLPFC tract analyses, including right AIns-NAcc tract coherence with functional activity in trial-to-trial prediction of incentivized inhibition performance improved the model's fit, and this extended model further predicted individual differences in incentivized inhibition in leave-one-subject-out cross validation (see Table 2). Again, increased right NAcc activity predicted reduced incentivized inhibition, but interestingly, modeling the interaction of right AIns-NAcc tract coherence with right NAcc activity revealed an interaction of right AIns-NAcc tract coherence with right NAcc activity to predict successful inhibition, consistent with an account in which AIns-NAcc tract coherence dampens NAcc activity to diminish approach behavior during incentivized inhibition (Leong et al., 2016).

Discussion

To characterize brain circuits that support incentivized inhibition, we combined a novel behavioral task with functional and structural neuroimaging. Behaviorally, incentives improved motor "go" responses, but impaired "no go" responses. Functionally, opposing patterns of brain activity in the right AIns and NAcc during anticipation of incentives predicted incentivized inhibition performance. Structurally, the coherence of a novel white-matter tract connecting the right AIns and VLPFC could account for individual differences in incentivized inhibition performance, as could the coherence of a tract connecting the right AIns and NAcc. A multimodal model integrating these findings revealed that greater right VLPFC activity statistically mediated the association of right AIns-VLPFC tract coherence with incentivized inhibition performance. These findings link previously disparate bodies of research on incentive anticipation and response inhibition to suggest that AIns projections can modulate VLPFC and NAcc activity in opposite directions to promote incentivized inhibition. Thus, while previous accounts of response inhibition have traditionally focused on the VLPFC, the current findings centrally implicate the upstream AIns as an important headwater for strengthening inhibition in the face of incentives.

To independently manipulate incentive anticipation and response inhibition on each trial, we developed a novel task (i.e., the "Monetary Incentive Delay Inhibition" or MIDI Task) in which individuals were instructed either to respond or not to respond to a motor target in order to obtain previously-cued monetary gains or avoid losses. As predicted, we found increased activity in mesolimbic circuits including the NAcc and AIns in response to incentive cues, but increased activity in cortical circuits including the VLPFC and DLPFC in response to inhibitory targets. Activity in these predicted regions combined to promote incentivized inhibition, such that NAcc activity decreased whereas AIns activity increased incentivized inhibition performance. These findings are consistent with the notion that while uncertain incentives may recruit many brain circuits, activity in different regions can have divergent implications for subsequent approach versus avoidance behavior (Knutson and Greer, 2008; Palminteri et al., 2012; Knutson and Huettel, 2015).

The MIDI task offers a new tool for dissociating neural and psychological processes that support incentivized inhibition by potentially distinguishing the motivation to obtain incentives from the inhibition of relevant motor responses. These findings suggest that AIns projections may diminish NAcc activity to prohibit appetitive impulses, while at the same time enhancing VLPFC activity to promote motor inhibition. Further, the timing of this predictive brain activity suggested that AIns responses to incentive cues preceded and so might modulate VLPFC responses to inhibitory targets. This temporal sequence is consistent with frameworks in which anticipatory affect precedes and can therefore modify subsequent processes related to value integration and motivation (Samanez-Larkin and Knutson, 2015), including inhibition of motor responses (Menon and Uddin, 2010). The temporal resolution of FMRI is limited, however, so other more invasive methods (e.g., electrophysiology) might better test temporal accounts only suggested by FMRI data. Future research might further causally establish the directionality of control between AIns and VLPFC circuits, and perhaps even structurally and functionally link them to additionally implicated DLPFC circuits.

In the current research, the MIDI Task was administered immediately after a more extensively-characterized incentive task (i.e., the MID task; Knutson et al., 2001) to potentiate a tendency towards motor responding. It is not clear whether such a procedure is necessary, or whether the MIDI task could be administered alone. Sequential ordering did afford direct comparison of neural responses to incentive cues across both tasks. Reassuringly, incorporating the motor inhibition component into the MIDI task did not quench neural responses to incentive cues – in fact, incentivized neural signals remained comparable or even slightly larger in the MIDI versus the MID task (see Supplementary Fig. 5). Further, neither behavioral performance nor brain activity in the preceding MID task could account for incentivized inhibition performance in the subsequent MIDI task, suggesting that the MIDI task could provide a uniquely informative neural probe of incentivized inhibition. Additional preregistered research will be necessary to establish whether the MIDI task can be administered alone, or must follow the MID task to invoke an interaction between incentives and inhibition.

With respect to behavior, the MIDI task is designed to present equal numbers of go and no go response targets (unlike traditional response inhibition tasks) in order to equally probe neural circuits that both incentivize and inhibit responses within the same task. Recent research suggests that in more traditional response inhibition tasks, equally balancing go and no go targets might reduce prepotent motor activity (e.g., Wessel, 2017), making responses more like considered choices than inhibited impulses. One implication of such a "considered choice" account is that incentives should slow responses. In the MIDI task, however, incentives helped "go" responses but hindered "no go" performance – apparently by speeding reaction times for both successful go and

unsuccessful no go responses (see Supplementary Fig. 2). Signal detection analyses confirmed that incentives had a suboptimal impact on performance, since incentive-induced decreases in response criterion were correlated with reduced task earnings overall (see Supplementary Fig. 3). Incentive-elicited brain activity also increased similarly prior to the subsequent appearance of go versus no go targets, suggesting that anticipatory activity did not solely index motor preparation (see Supplementary Fig. 4).

With respect to brain function, recently-developed response inhibition neuroimaging tasks have varied incentives as well as inhibition demands, but have not separately manipulated incentive and inhibition instructions on a trial-to-trial basis (e.g., Leotti and Wager, 2010; Guitart-Masip et al., 2012). For instance, a relevant learning task tested an ethological account in which gain incentives potentiate go responses, but loss incentives instead potentiate no go responses (Guitart-Masip et al., 2012). In the present research, however, both gain and loss incentives enhanced go responses while impairing no go responses. These different results may depend on task design. In the dynamic learning task described above, incentive and inhibitory instructions were simultaneously presented during the cue period, whereas in the current static MIDI task, incentive cues reliably preceded inhibitory targets. Similarly, eye movement tasks have presented both incentive and inhibitory instructions during the cue period, but find that incentives promote rather than prohibit inhibitory responses (e.g., Jazbec et al., 2006). Although different designs may yield divergent results, the MIDI task clearly and reproducibly elicits conditions under which incentives can impair inhibitory performance, in sharp contrast to standard economic accounts in which incentives should increase optimal performance (Ariely et al., 2009). This reliable elicitation of incentivized inhibition may position the MIDI task as a useful probe of behavior and brain function in the context of impulse control disorders.

With respect to brain structure, predictions inspired by comparative neuroanatomical research not only guided the present attempts to replicate evidence for a tract connecting the AIns to the NAcc, but also to further characterize a novel tract connecting the AIns and the VLPFC. While the coherence of both tracts was associated with individual differences in incentivized inhibition performance, different coherence metrics were related to behavior in the two tracts. Conceptually extending previous work on preferences against lottery-like (or positively-skewed) gambles, fractional anisotropy (FA) of the right AIns-NAcc tract positively correlated with individual differences in incentivized inhibition performance (whereas inverse MD only showed a trend towards this association; Leong et al., 2016). For the right AIns-VLPFC tract, however, inverse mean diffusivity (MD) positively correlated with individual differences in incentivized inhibition performance (but not FA). The AIns-VLPFC tract travels closer to the cerebral cortex, which might involve more complex or numerous fiber crossings (Vos et al., 2010). This association is also consistent with previous evidence that white matter coherence near the tract's VLPFC projection terminal correlates with functional brain activity and performance in a response inhibition task (Forstmann et al., 2008). Histological comparative research might eventually clarify why different tract coherence metrics correlate with brain activity and behavioral performance in distinct circuits. Importantly, the observed associations were specific to the predicted tracts and did not extend to qualities of other potentially relevant tracts, including tracts traditionally associated with motor inhibition (e.g., those connecting the pre-supplementary motor area (preSMA) and subthalamic nucleus (STN), MPFC and NAcc, or VLPFC and STN; see full characterization in Materials and Methods, Supplementary Fig. 6, and Supplementary Table 6). Recent primate tract tracing studies suggest that projections from parietal cortex and more posterior ventrolateral cortex converge in the striatum (Choi et al., 2017), but these join in more dorsal zones than ventral striatal targets explored in the current research (i.e., near the NAcc).

Technical advances continue to increase the spatial and temporal resolution of neuroimaging probes of brain structure and function, but methods for combining these multimodal probes to predict behavior on a trial-to-trial basis are lacking. While measures of brain structure can assess differences between individuals, measures of brain activity can better track second-to-second variability within individuals. In future research, structural measures might inform priors which can then constrain and sharpen functional measures (Grosenick et al., 2013). Although theorists have recently suggested that structural connectivity implies functionally correlated activity (Honey et al., 2009), in the current research, functional correlations of activity in connected regions of interest did not significantly vary by experimental condition, and were also not associated with task performance (see Supplementary Fig. 8). Links between structure and function may eventually reveal more specific physiological principles that can clarify how structural projections support functional signaling between brain regions, and also might highlight circuit targets for causal manipulations using precise techniques in animal models (Ferenczi et al., 2016; Stauffer et al., 2016). Thus, by bridging brain structure and function, researchers might build more constrained but complete models of how neuroimaging signals flow through interconnected circuits to promote behavior (Haber and Knutson, 2010; Chang et al., 2013; Samanez-Larkin and Knutson, 2015).

By linking levels of analysis, research might inspire more targeted interventions for psychiatric symptom profiles related to poor incentivized inhibition, including drug addiction and impulse control disorders (Koob and Volkow, 2010). The present findings fit with observations that right VLPFC white matter coherence is diminished in individuals who have abused stimulants – and that these individuals also show performance deficits in response inhibition (Ersche et al., 2012). Perhaps their symptomatic deficits in response inhibition are most pronounced particularly when they should not be – in the face of significant incentives. These findings further imply that anticipatory affect can modulate motor output – both when that output should be promoted but also when it must be prohibited. By tracking multimodal changes in the structure and function of incentivized inhibition circuits over time, researchers might better understand how people can not only lose but also eventually gain control over even the most powerful of impulses.

Author contributions

B.K., G.R.S.L., and J.K.L. designed the research. G.R.S.L., J.K.L., and K.H.M. acquired the data. B.K. and J.K.L. analyzed the data. All authors wrote the paper.

Acknowledgments

We thank Tim Behrens, Patrick Bissett, Marc Guitart-Masip, Russell Poldrack, Elliott Wimmer, and spanlab for helpful comments on the manuscript. We also thank Emily Jensen, Kiefer Katovich, and Charlene Wu for assistance in collecting data. This research was supported by a Stanford Neuroscience Institute NeuroChoice Initiative grant to Brian Knutson. Josiah Leong was supported by the National Institute of Mental Health Predoctoral Training Program (T32-MH020006). Kelly MacNiven was supported by the NeuroChoice Initiative postdoctoral fellowship. Gregory Samanez-Larkin was supported by the National Institute on Aging (F32-AG039131, K99-AG0425696, R00-AG042596).

Appendix A. Supplementary data

Supplementary data related to this article can be found at https://doi.org/10.1016/j.neuroimage.2018.05.055.

References

Ariely, D., Gneezy, U., Loewenstein, G., Mazar, N., 2009. Large stakes and big mistakes. Rev. Econ. Stud. 76, 451–469.

Aron, A.R., Fletcher, P.C., Bullmore, E.T., Sahakian, B.J., Robbins, T.W., 2003. Stop-signal inhibition disrupted by damage to right inferior frontal gyrus in humans. Nat. Neurosci. 6, 115–116.

Aron, A.R., Poldrack, R.A., 2006. Cortical and subcortical contributions to stop signal response inhibition: role of the subthalamic nucleus. J. Neurosci. 26, 2424–2433.
Aron, A.R., Behrens, T.E., Smith, S., Frank, M.J., Poldrack, R.A., 2007. Triangulating a cognitive control network using diffusion-weighted magnetic resonance imaging (MRI) and functional MRI. J. Neurosci. 27, 3743–3752.
Basser, P.J., Pierpaoli, C., 1996. Microstructural and physiological features of tissues elucidated by quantitative-diffusion-tensor MRI. J. Magn. Reson. B 111, 209–219.
Boekel, W., Forstmann, B.U., Keuken, M.C., 2017. A test-retest reliability analysis of diffusion measures of white matter tracts relevant for cognitive control. Psychophysiology 54, 24–33.
Cai, W., Ryali, S., Chen, T., Li, C.S.R., Menon, V., 2014. Dissociable roles of right inferior frontal cortex and anterior insula in inhibitory control: evidence from intrinsic and task-related functional parcellation, connectivity, and response profile analyses across multiple datasets. J. Neurosci. 34, 14652–14667.
Cerliani, L., Thomas, R.M., Jbabdi, S., Siero, J.C.W., Nanetti, L., Crippa, A., Gazzola, V., D'Arceuil, H., Keysers, C., 2011. Probabilistic tractography recovers a rostrocaudal trajectory of connectivity variability in the human insular cortex. Hum. Brain Mapp. 33, 2005–2034.
Chang, L.J., Yarkoni, T., Khaw, M.W., Sanfey, A.G., 2013. Decoding the role of the insula in human cognition: functional parcellation and large-scale reverse inference. Cerebr. Cortex 23, 739–749.
Chang, E.H., Argyelan, M., Aggarwal, M., Chandon, T.S., Karlsgodt, K.H., Mori, S., Malhotra, A.K., 2017. The role of myelination in measures of white matter integrity: combination of diffusion tensor imaging and two-photon microscopy of CLARITY intact brains. Neuroimage 147, 253–261.
Chikama, M., McFarland, N.R., Amaral, D.G., Haber, S.N., 1997. Insular cortical projections to functional regions of the striatum correlate with cortical cytoarchitectonic organization in the primate. J. Neurosci. 17, 9686–9705.
Choi, E.Y., Tanimura, Y., Vage, P.R., Yates, E.H., Haber, S.N., 2017. Convergence of prefrontal and parietal anatomical projections in a connectional hub in the striatum. Neuroimage 146, 821–832.
Cloutman, L.L., Binney, R.J., Drakesmith, M., Parker, G.J.M., Lambon Ralph, M.A., 2011. The variation of function across the human insula mirrors its patterns of structural connectivity: evidence from in vivo probabilistic tractography. Neuroimage 59, 3514–3521.
Cohen, M.S., 1997. Parametric analysis of fMRI data using linear systems methods. Neuroimage 6, 93–103.
Desikan, R.S., et al., 2006. An automated labeling system for subdividing the human cerebral cortex on MRI scans into gyral based regions of interest. Neuroimage 31, 968–980.
Destrieux, C., Fischl, B., Dale, A., Halgren, E., 2010. Automatic parcellation of human cortical gyri and sulci using standard anatomical nomenclature. Neuroimage 53, 1–15.
Dunovan, K., Lynch, B., Molesworth, T., Verstynen, T., 2015. Competing basal ganglia pathways determine the difference between stopping and deciding not to go. eLife 4, e08723.
Ersche, K.D., Simon Jones, P., Williams, G.B., Turton, A.J., Robbins, T.W., Bullmore, E.T., 2012. Abnormal brain structure implicated in stimulant drug addiction. Science 335, 601–604.
Ferenczi, E.A., et al., 2016. Prefrontal cortical regulation of brainwide circuit dynamics and reward-related behavior. Science 351 aac9698.
Fischl, B., et al., 2004. Automatically parcellating the human cerebral cortex. Cerebr. Cortex 14, 11–22.
Forstmann, B.U., Jahfari, S., Steven Scholte, H., Wolfensteller, U., van den Wildenberg, W.P.M., Richard Ridderinkhof, K., 2008. Function and structure of the right inferior frontal cortex predict individual differences in response inhibition: a model-based approach. J. Neurosci. 28, 9790–9796.
Gomez, J., Pestilli, F., Witthoft, N., Golarai, G., Liberman, A., Poltoratski, S., Yoon, J., Grill- Spector, K., 2016. Functionally defined white matter reveals segregated pathways in human ventral temporal cortex associated with category-specific processing. Neuron 85, 216–227.
Graybiel, A., 1990. Neurotransmitters and neuromodulators in the basal ganglia. Trends Neurosci. 13, 244–253.
Grosenick, L., Klingenberg, B., Katovich, K., Knutson, B., Taylor, J.E., 2013. Interpretable whole brain prediction analysis with GraphNet. Neuroimage 72, 304–321.
Guitart-Masip, M., Huys, Q.J.M., Fuentemilla, L., Dayan, P., Duzel, E., Dolan, R.J., 2012. Go and no- go learning reward and punishment: interactions between affect and effect. Neuroimage 62, 154–166.
Haber, S.N., Knutson, B., 2010. The reward circuit: linking primate anatomy and human imaging. Neuropsychopharmacology 35, 4–26.
Honey, C.J., Sporns, O., Cammoun, L., Gigandet, X., Thiran, J.P., Meuli, R., Hagmann, P., 2009. Predicting human resting-state functional connectivity from structural connectivity. Proc. Natl. Acad. Sci. U.S.A. 106, 2035–2040.
Jazbec, S., Hardin, M.G., Schroth, E., McClure, E., Pine, D.S., Ernst, M., 2006. Age-related influence of contingencies on a saccade task. Exp. Brain Res. 174, 754–762.
Jbabdi, S., Sotiropoulos, S.N., Haber, S.N., Van Essen, D.C., Behrens, T.E., 2015. Measuring macroscopic brain connections in vivo. Nat. Neurosci. 18, 1546–1555.
Johansen-Berg, H., Behrens, T.E.J., Robson, M.D., Drobnjak, I., Rushworth, M.F.S., Brady, J.M., Smith, S.M., Higham, D.J., Matthews, P.M., 2004. Changes in connectivity profiles define functionally distinct regions in human medial frontal cortex. Proc. Natl. Acad. Sci. U.S.A. 101, 13335–13340.
Jones, D.K., Knosche, K.R., Turner, R., 2013. White matter integrity, fiber count, and other fallacies: the do's and don'ts of diffusion MRI. Neuroimage 73, 239–254.
Knutson, B., Adams, C.S., Fong, G.W., Hommer, D., 2001. Anticipation of monetary reward selectively recruits nucleus accumbens. J. Neurosci. 21. RC159.
Knutson, B., Greer, S.M., 2008. Anticipatory affect: neural correlates and consequences for choice. Philos. Trans. R Soc. Lond. B Biol. 363, 3771–3786.
Knutson, B., Huettel, S.A., 2015. The risk matrix. Curr. Opin. Behav. Sci. 5, 141–146.
Koob, G.F., Volkow, N.D., 2010. Neurocircuitry of addiction. Neuropsychopharmacology 35, 217–238.
Lehman, J.F., Greenberg, B.D., McIntyre, C.C., Rasmussen, S.A., Haber, S.N., 2011. Rules ventral prefrontal cortical axons use to reach their targets: implications for diffusion tensor imaging tractography and deep brain stimulation for psychiatric illness. J. Neurosci. 31, 10392–10402.
Leong, J.K., Pestilli, F., Wu, C.W., Samanez-Larkin, G.R., Knutson, B., 2016. White-matter tract connecting anterior insula to nucleus accumbens correlates with reduced preference for positively skewed gambles. Neuron 89, 63–69.
Leotti, L.A., Wager, T.D., 2010. Motivational influences on response inhibition. J. Exp. Psychol. Hum. Percept. Perform. 36, 430–447.
Levy, B.J., Wagner, A.D., 2011. Cognitive control and right ventrolateral prefrontal cortex: reflexive reorienting, motor inhibition, and action updating. Ann. N. Y. Acad. Sci. 1224, 40–62.
Menon, V., Uddin, L.Q., 2010. Saliency, switching, attention and control: a network model of insula function. Brain Struct. Funct. 214, 655–667.
Mesulam, M.M., Mufson, E.J., 1982. Insula of the old world monkey. III: efferent cortical output and comments on function. J. Comp. Neurol. 212, 38–52.
Mogenson, G.J., Jones, D.L., Yim, C.Y., 1980. From motivation to action: functional interface between the limbic system and the motor system. Prog. Neurobiol. 14, 69–97.
Mufson, E.J., Mesulam, M.M., 1982. Insula of the old world monkey. II: afferent cortical input and comments on the claustrum. J. Comp. Neurol. 212, 23–37.
O'Connor, D.A., Rossiter, S., Yücel, M., Lubman, D.I., Hester, R., 2012. Successful inhibitory control over an immediate reward is associated with attentional disengagement in visual processing areas. Neuroimage 62, 1841–1847.
Padmala, S., Pessoa, L., 2010. Interactions between cognition and motivation during response inhibition. Neuropsychologia 48, 558–565.
Palminteri, S., Justo, D., Jauffer, C., Pavlicek, B., Dauta, A., Delmaire, C., Czernecki, V., Karachi, C., Capelle, L., Durr, A., Pessiglione, M., 2012. Critical roles for anterior insula and dorsal striatum in punishment-based avoidance learning. Neuron 76, 998–1009.
Pestilli, F., Yeatman, J.D., Rokem, A., Kay, K.N., Wandell, B.A., 2014. Evaluation and statistical inference for human connectomes. Br. J. Pharmacol. 11, 1058–1063.
Petrides, M., Pandya, D.N., 2001. Comparative cytoarchitectonic analysis of the human and the macaque ventrolateral prefrontal cortex and corticocortical connection patterns in the monkey. Eur. J. Neurol. 16, 291–310.
Rae, C.L., Hughes, L.E., Anderson, M.C., Rose, J.B., 2015. The prefrontal cortex achieves inhibitory control by facilitating subcortical motor pathway connectivity. J. Neurosci. 35, 786–794.
Reynolds, S.M., Zahm, D.S., 2005. Specificity in the projections of prefrontal and insular cortex to ventral striatopallidum and the extended amygdala. J. Neurosci. 25, 11757–11767.
Robbins, T.W., Everitt, B.J., 1996. Neurobehavioural mechanisms of reward and motivation. Curr. Opin. Neurobiol. 6, 228–236.
Rudebeck, P.H., Saunders, R.C., Lundgren, D.A., Murray, E.A., 2017. Specialized representations of value in the orbital and ventrolateral prefrontal cortex: desirability versus availability of outcomes. Neuron 95, 1208–1220.
Samanez-Larkin, G.R., Levens, S.M., Perry, L.M., Dougherty, R.F., Knutson, B., 2012. Frontostriatal white matter integrity mediates adult age differences in probabilistic reward learning. J. Neurosci. 32, 5333–5337.
Samanez-Larkin, G.R., Knutson, B., 2015. Decision making in the ageing brain: changes in affective and motivational circuits. Nat. Rev. Neurosci. 16, 278–289.
Sherbondy, A.J., Dougherty, R.F., Ben-shachar, M., Wandell, B.A., 2008. ConTrack: finding the most likely pathways between brain regions using diffusion tractography. J. Vis. 8, 1–16.
Stauffer, W.R., Lak, A., Yang, A., Borel, M., Paulsen, O., Boyden, E.S., Schultz, W., 2016. Dopamine neuron-specific optogenetic stimulation in rhesus macaques. Cell 166, 1564–1571 e6.
Swick, D., Ashley, V., Turken, U., 2011. Are the neural correlates of stopping and not going identical? Quantitative meta-analysis of two response inhibition tasks. Neuroimage 56, 1655–1665.
Tournier, J.D., Calamante, F., Connelly, A., 2007. Robust determination of the fibre orientation distribution in diffusion MRI: non-negativity constrained super-resolved spherical deconvolution. Neuroimage 35, 1459–1472.
Vos, S.B., Jones, D.K., Jeurissen, B., Viergever, M.A., Leemans, A., 2010. The influence of complex white matter architecture on the mean diffusivity in diffusion tensor MRI of the human brain. Neuroimage 59, 2208–2216.
Wessel, J.R., 2017. Prepotent motor activity and inhibitory control demands in different variants of the go/no-go paradigm. Psychophysiology. https://doi.org/10.1111/psyp.12871. Advanced Online Publication.
Wu, C.C., Samanez-Larkin, G.R., Katovich, K., Knutson, B., 2014. Affective traits link to reliable neural markers of incentive anticipation. Neuroimage 84, 279–289.
Yeatman, J.D., Dougherty, R.F., Myall, N.J., Wandell, B.A., Feldman, H.M., 2012. Tract profiles of white matter properties: automating fiber-tract quantification. PLoS One 7, e49790.

Supplementary Materials

Supplementary Figure 1. Statistical collinearity analyses of regressors of interest in whole brain analysis

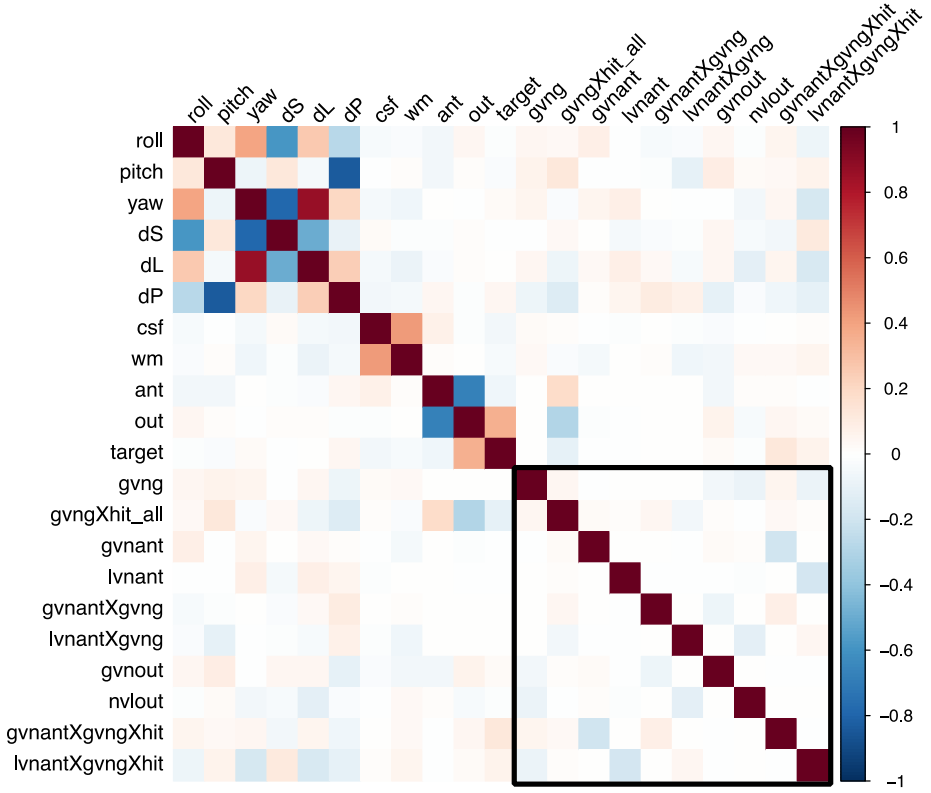

	gvng	gvng Xhit_all	gvnant	lvnant	gvnant Xgvng	lvnant Xgvng	gvnout	nvlout	gvnant XgvngXhit
gvng	1								
gvngXhit_all	0.154	1							
gvnant	–0.001	0.028	1						
lvnant	0.004	0.017	0	1					
gvnantXgvng	0	0.109	0.001	–0.001	1				
lvnantXgvng	0	0.022	–0.002	–0.001	0	1			
gvnout	–0.165	0.059	0.022	–0.003	–0.234	0	1		
nvlout	–0.219	0.059	0.013	0.029	0	–0.311	–0.014	1	
gvnantXgvngXhit	0.148	0.031	–0.299	0.001	0.125	0	–0.007	–0.007	1
lvnantXgvngXhit	0.029	0.01	–0.001	–0.339	0	0.292	–0.002	–0.003	–0.001

A representative design matrix of a single subject, which also includes eleven regressors of no interest for six axes of motion, control activity in cerebrospinal fluid and white matter, and period regressors for incentive anticipation, target response, and trial outcome. Collinearity analysis of the experimental design matrix verifies the independence of the regressors of interest (outlined in black in the correlation matrix). Importantly, the regressor for go versus no go targets was statistically independent of both gain versus non-gain anticipation (r = –0.001) and loss versus non-loss anticipation (r = 0.004), consistent with the balanced factorial design of the MIDI task.

Supplementary Figure 2. Split-half and reaction time analyses of behavioral performance.

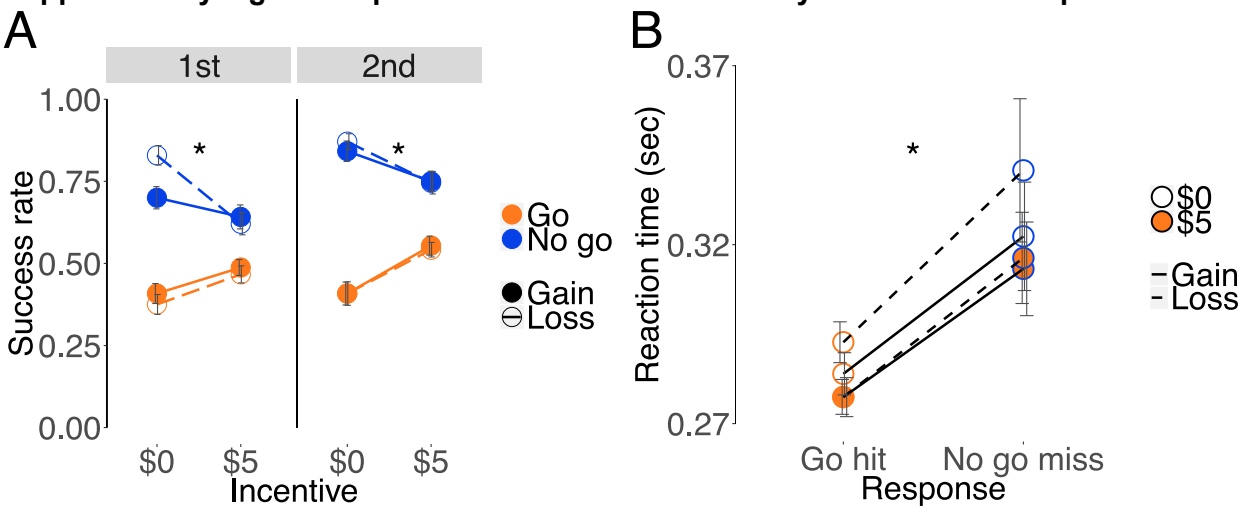

(**A**) Incentives improved motor "go" performance and impaired inhibitory "no go" performance in both halves of the experiment (+/–$5 versus +/–$0 go first half: paired t(39) = 3.41, p = 0.002; second half: paired t(39) = 5.15, p < 0.0001; +/–$5 versus +/–$0 no go first half: paired t(39) = -3.65, p < 0.001; second half: paired t(39) = –3.61, p < 0.001). However individuals' performance improved during the second half of the experiment, particularly for inhibition (+/–$5 go: paired t(39) = –2.24, p = 0.03; +/–$5 no go: paired t(39) = 4.20, p < 0.001; +/–$0 go: paired t(39) = 0.46, p = 0.65; +/–$0 no go: paired t(39) 4.11, p < 0.001). An adaptive algorithm dynamically adjusted the reaction time necessary to achieve a targeted 66% hit rate within “go” conditions, but not “no go” conditions (which might account for improvement during the second half of the task in "no go" conditions).

Since improvements in inhibitory performance during the second half of the task were not predicted, we separately tested associations between incentivized inhibition performance and individual differences in brain measures for each half of the task. Right AIns-NAcc tract coherence (FA) was associated with first half incentivized inhibition performance at trendwise significance (β = 0.31, t(38) = 1.99, p = 0.054), and was significantly associated with second half performance (β = 0.33, t(38) = 2.15, p = 0.038). Right AIns-VLPFC tract coherence (1-MD) was not significantly associated with first half performance (β = 0.18, t(38) = 1.12, p = 0.27), but was significantly associated with second half performance (β = 0.51, t(38) = 3.68, p < 0.001). During both halves of the task, incentivized inhibition was associated with right VLPFC functional activity (first half: β = 0.33, t(38) = 2.18, p = 0.036; second half: β = 0.38, t(38) = 2.56, p = 0.015).

(**B**) Incentives sped reaction times for both successful "go" responses and unsuccessful “no go” responses across all conditions (paired t(30) = –2.06, p = 0.048). Within each condition, reaction times were slower when individuals failed to inhibit responses than when the individuals successfully responded to "go" targets (+$5: paired t(38) = 3.11, p = 0.004; –$5: paired t(38) = 2.89, p = 0.006; +$0: t(34) = 2.38, p = 0.023; –$0: t(31) = 2.07, p = 0.047). Different degrees of freedom in each paired t-test resulted in different numbers of subjects with reaction time data for each relevant condition.

Supplementary Figure 3. Signal detection theory analysis of behavior

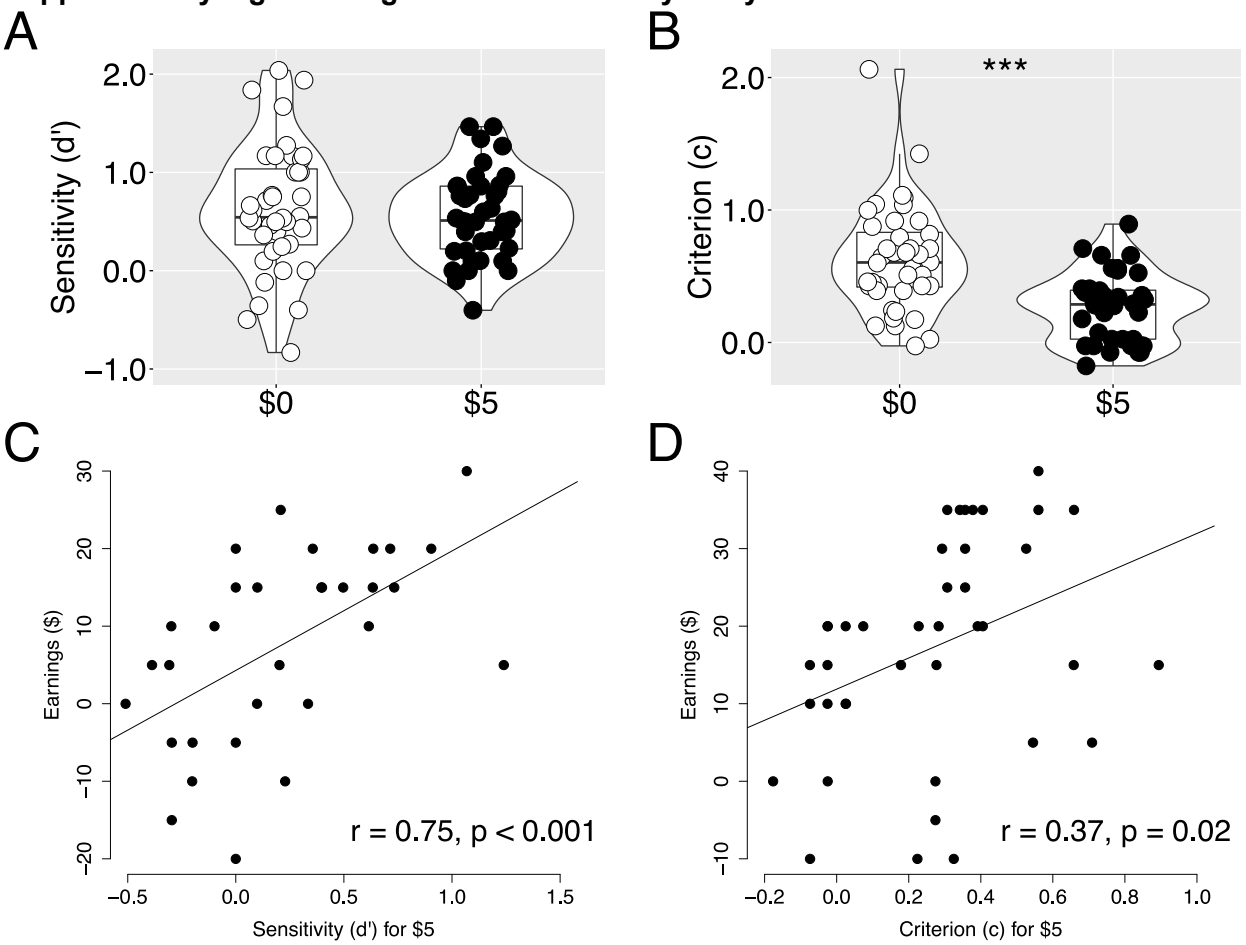

(A, B) Signal detection analysis was conducted on the behavioral performance data for incentivized (+/–$5) and non-incentivized trials (+/–$0). Incentives did not influence sensitivity of responding (d-prime; paired $t(39) = –0.75$, $p = 0.46$); but did decrease the criterion (c) for responding (thus lowering the response threshold; paired $t(39) = –5.12$, $p < 0.001$).

(C, D) Both increased sensitivity and increased criterion for incentivized trials were associated with greater earnings in the MIDI Task (d-prime: $r = 0.75$, $p < 0.001$; c: $r = 0.37$, $p = 0.02$).

Since increased criterion indicates a higher threshold for performing a “go” response and is also associated with greater earnings, these findings suggest that incentives decreased the response threshold, and so reduced subjects’ earnings in the MIDI Task.

Supplementary Figure 4. Brain activity for loss incentive trials.

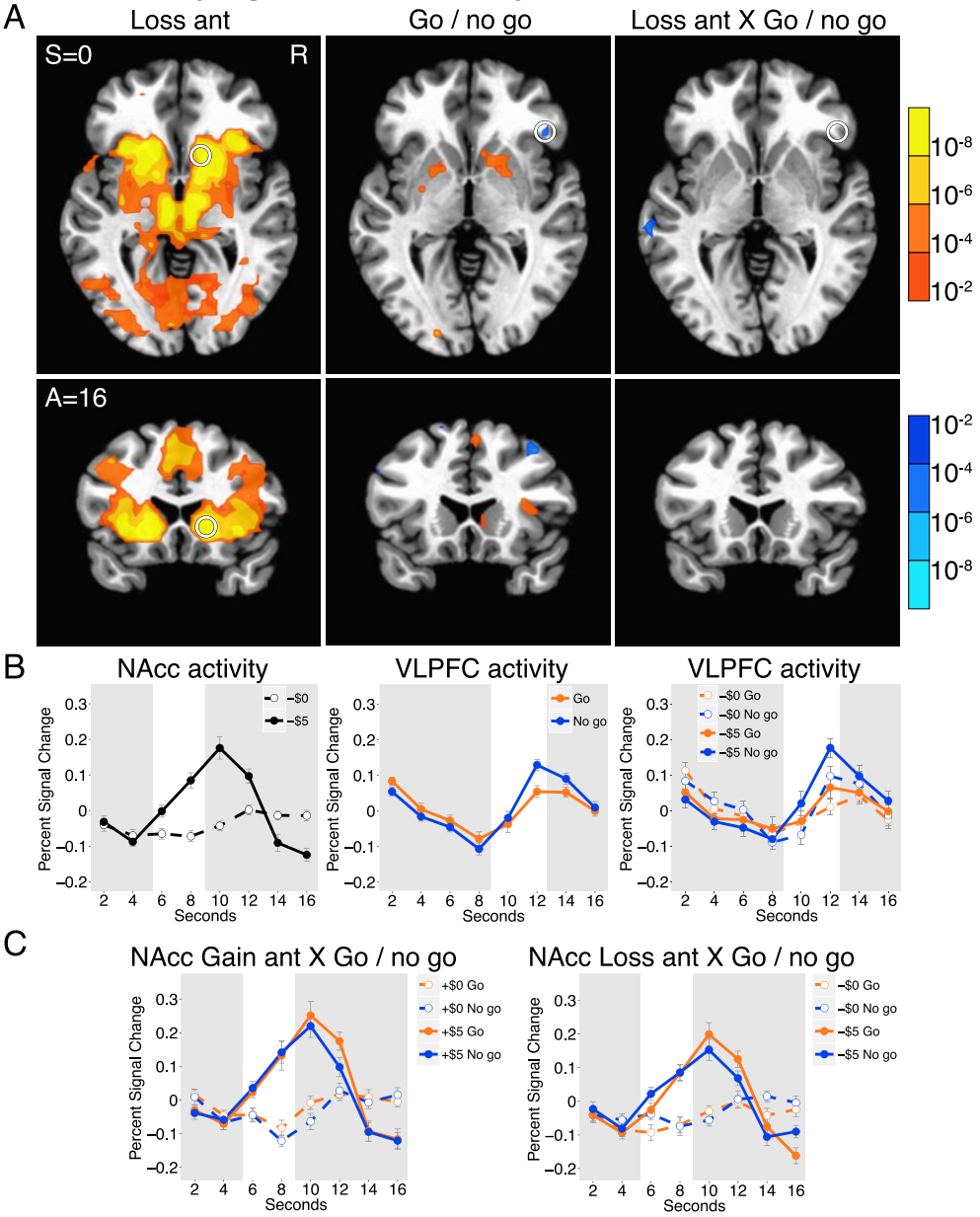

(**A**) Contrast maps depict the main effects of anticipating losses versus non-losses (Loss ant), go versus no go responses (Go / no go), and their interaction (Loss ant X Go / no go) on brain activity. Warm colors indicate increased activity while cool colors indicate decreased activity for relevant contrasts (R = right; A = anterior; S = superior). Maps were thresholded voxelwise $p < 0.001$, and cluster corrected $p < 0.05$, as in the main text.

(**B**) Averaged activity time courses extracted from volumes of interest show increased NAcc activity during anticipation of loss versus non-loss, and greater right VLPFC activity in response to no go versus go targets.

(**C**) Averaged activity time courses extracted from volumes of interest show increased NAcc activity for gain versus loss anticipation cues, but no difference in response to presentation of "go" versus "no go" targets (+$5: paired $t(39) = 0.28$, $p = 0.78$; +$0: paired $t(39) = –1.36$, $p = 0.18$; –$5: paired $t(39) = 0.07$, $p = 0.94$; –$0: paired $t(39) = –0.12$, $p = 0.91$), indicating that NAcc anticipatory activity responded to incentive cues but not inhibitory targets.

Supplementary Figure 5. Comparison of incentive-elicited brain activity in the MID versus MIDI Tasks.

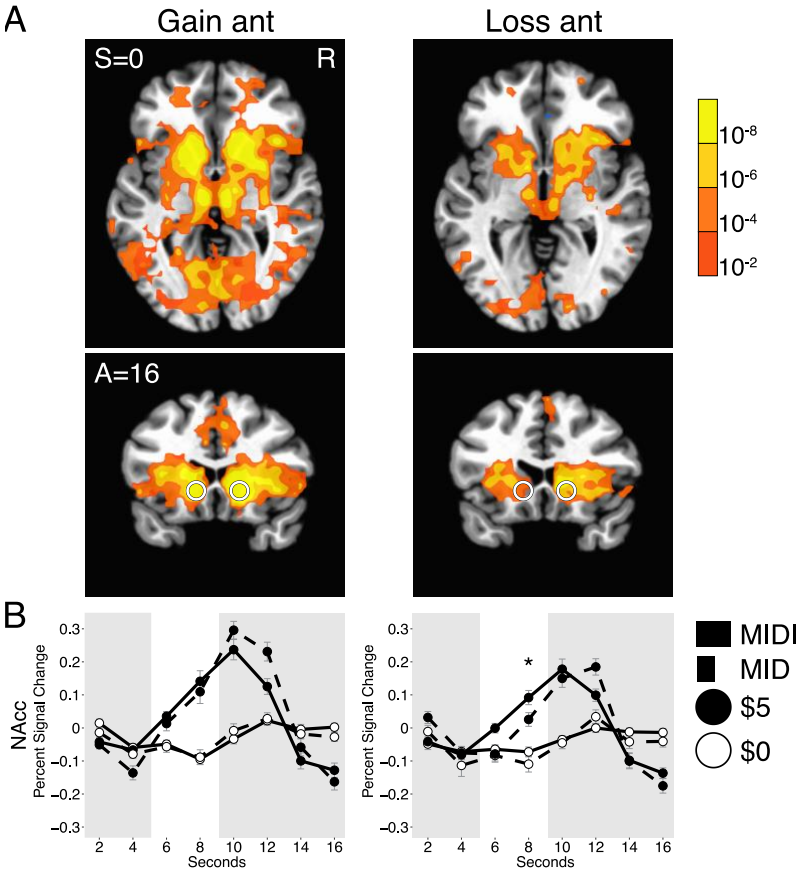

(**A**) Whole-brain maps (z-score transformed) contrasting anticipation of large gains versus non-gains (Gain ant), and large losses versus non-losses (Loss ant) during the monetary incentive delay (MID) task (performed immediately before the MIDI task). MID contrast maps reveal similar patterns of brain activity as equivalent contrasts in the MIDI task (see Figure 2 and Supplementary Figure 4). Maps were thresholded as in the main text for the MIDI task, voxelwise $p < 0.001$, with a minimum cluster size of five 3 mm cubic voxels (S = superior; A = anterior; R = right).

(**B**) Activity time courses extracted from NAcc VOIs (as described in the main text) during gain anticipation were similar across MID and MIDI Tasks (gain both NAcc: paired $t(39) = 0.86$, $p = 0.39$; loss both NAcc: paired $t(39) = 3.14$; $p = 0.003$).

Behavioral performance and functional activity in the MID task were not significantly associated with incentivized inhibition performance in the MIDI task (+$5 MID hit rate: $\beta = -0.28$, $t(38) = -1.83$, $p = 0.08$; –$5 MID hit rate: $\beta = -0.22$, $t(38) = v1.39$, $p = 0.17$; +$5 NAcc: $\beta = 0.09$, $t(38) = 0.53$, $p = 0.60$; –$5 NAcc: $\beta = 0.20$, $t(38) = 1.27$, $p = 0.21$; +$5 AIns: $\beta = 0.02$, $t(38) = 0.10$, $p = 0.92$; –$5 AIns: $\beta = 0.19$, $t(38) = 1.20$, $p = 0.24$; +$5 VLPFC: $\beta = -0.07$, $t(38) = -0.44$, $p = 0.6$; –$5 VLPFC: $\beta = 0.06$, $t(38) = 0.38$, $p = 0.71$). However, individual differences in successful go performance to avoid losing $5 and to avoid losing $0 in the MID task were positively associated with performance in equivalent conditions in the MIDI task, although only the second association passed corrected significance thresholds for multiple tests (–$5 go: $\beta = 0.32$, $t(38) = 2.06$, $p = 0.047$; –$0 go: $\beta = 0.46$, $t(38) = 3.15$, $p = 0.003$; * $p < 0.05$).

Supplementary Figure 6. Tracing and validation of control tracts.

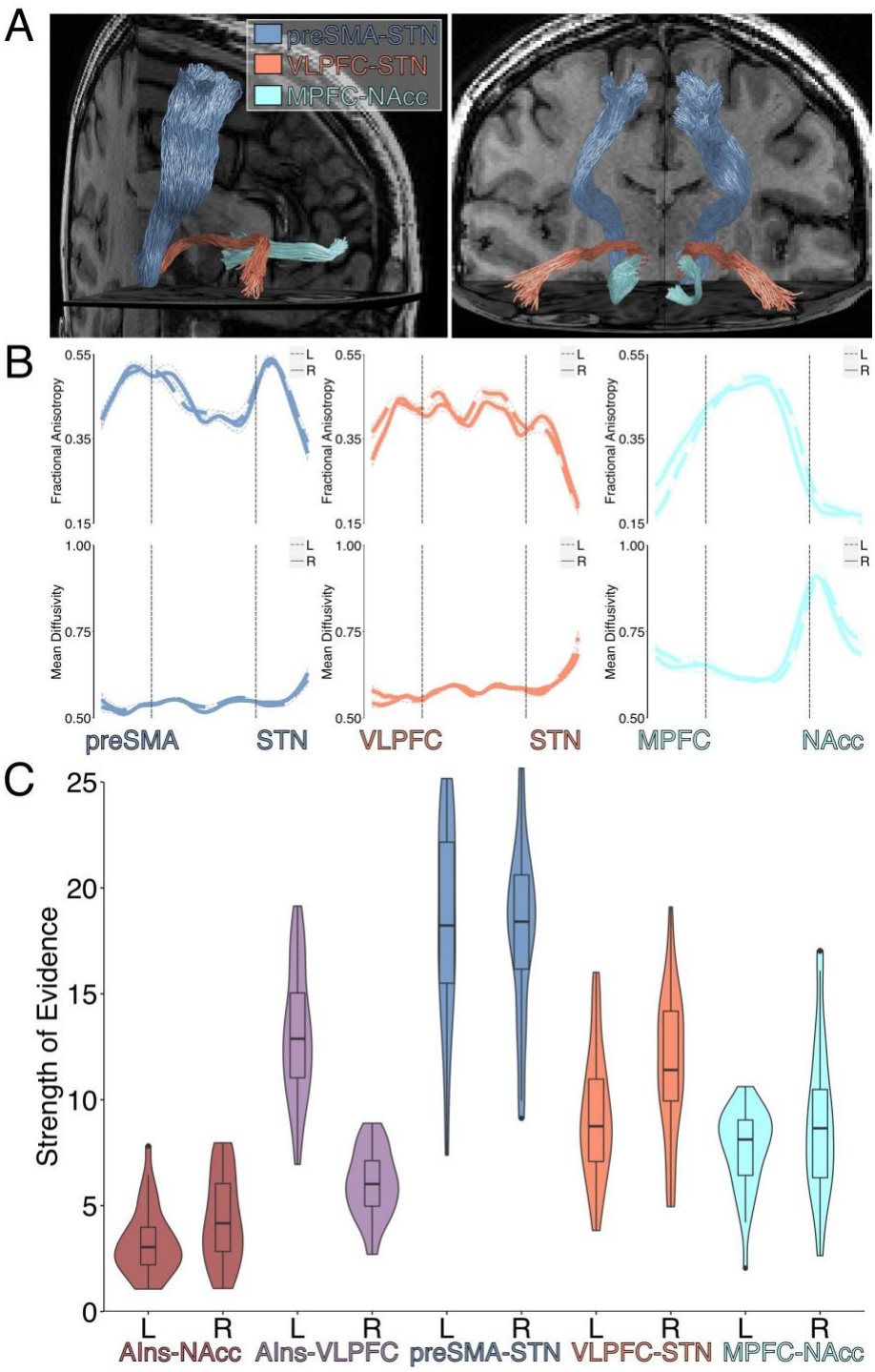

(**A**) Control tracts were traced between the presupplementary motor area (preSMA) and the subthalamic nucleus (STN), VLPFC and STN, and MPFC and NAcc. The preSMA-STN and VLPFC-STN tracts were traced using the same method as the tracts of interest in the main text (see Materials and Methods). The MPFC-NAcc tract was traced using previously reported methods (Samanez-Larkin et al., 2012).

(**B**) Tract coherence profiles display fractional anisotropy and mean diffusivity along the trajectory of each tract for each hemisphere (mean with standard errors). The middle 50% of each tract was averaged to obtain a value to include as covariates of no interest in regression analyses (see Supplementary Table 6).

(**C**) Linear fascicle evaluation (LIFE) with virtual lesions was performed to assess the evidence for the existence of each tract (Pestilli et al., 2014). Violin plots depict the evidence for each tract in each hemisphere of every subject. These scores were log-transformed to unbound the distribution at zero, and t-tests were performed to test group-wise evidence for each tract of interest against a null value of zero (Leong et al., 2016). Results indicate that each tract of interest incrementally improved prediction of the raw diffusion data relative to the whole-brain connectome, and thus statistically supported the presence of each bilateral tract.

Supplementary Figure 7. Tracts of interest in representative subjects.
Depiction of four subjects' right hemisphere AIns-NAcc and AIns-VLPFC tracts, as well as bilateral preSMA-STN, VLPFC-STN, and MPFC-NAcc tracts. All tracts followed a similar trajectory in every subject.

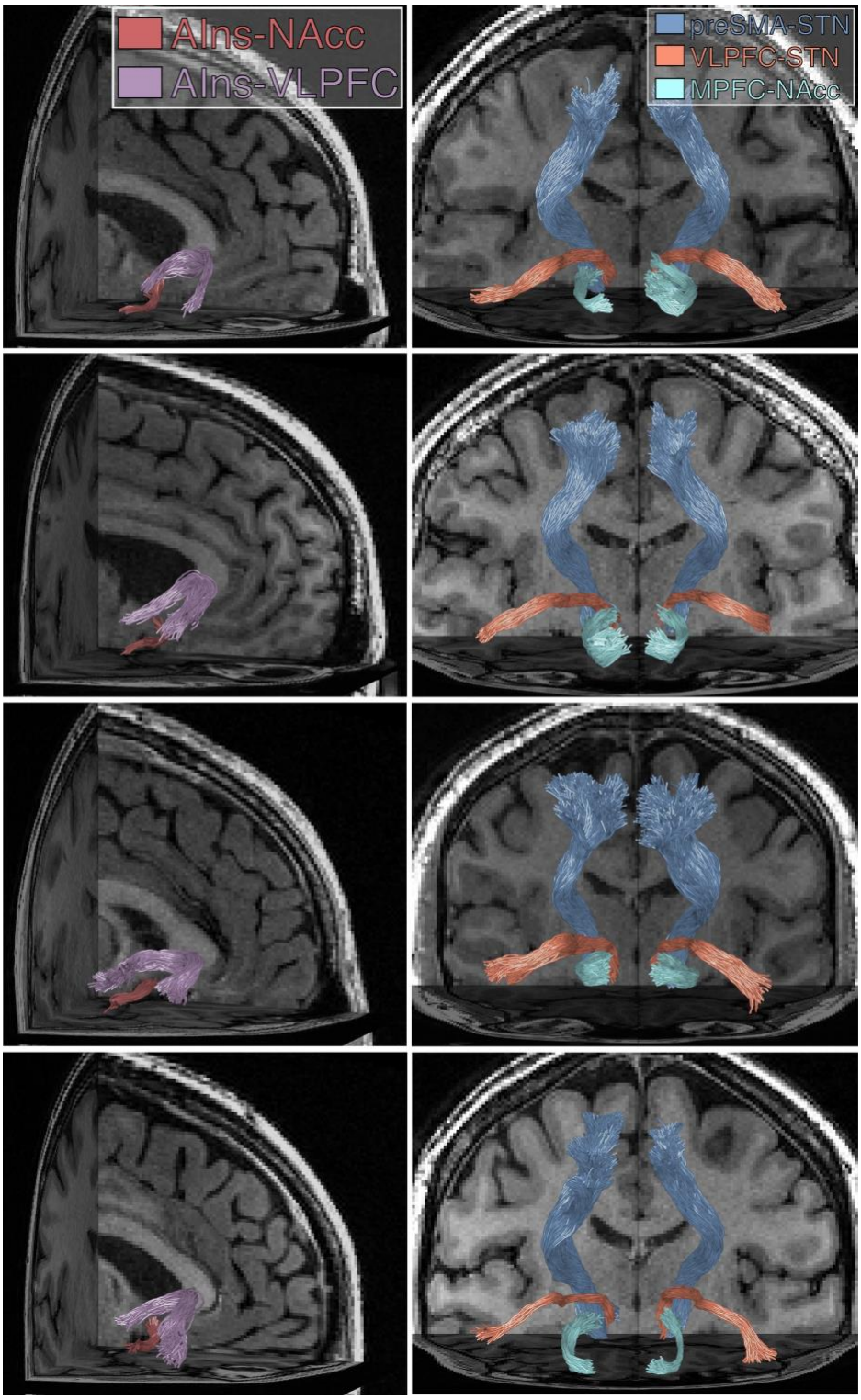

We assessed test-rested reliability of tract coherence measures in all tracts in a separate sample (n = 7). Subjects were scanned twice using the same diffusion-weighted MRI sequence as in the present study. Tracts were traced and tract coherence was estimated in each scan as described in the present study. Tract coherence measures (FA and inverse MD) exhibited high test-retest reliability for all tracts except for the preSMA-STN tract.

Intraclass correlations:
AIns-NAcc FA
ICC2k = 0.96, $p < 0.01$
AIns-NAcc MD
ICC2k = 0.99, $p < 0.01$
AIns-VLPFC FA:
ICC2k = 0.95, $p < 0.01$
AIns-VLPFC MD:
ICC2k = 0.84, $p < 0.05$
preSMA-STN FA
ICC2k = 0.71, $p = 0.08$
preSMA-STN MD
ICC2k = 0.23, $p = 0.40$
VLPFC-STN FA
ICC2k = 0.90, $p < 0.05$
VLPFC-STN MD:
ICC2k = 0.93, $p < 0.01$
MPFC-NAcc FA
ICC2k = 0.97, $p < 0.01$
MPFC-NAcc MD:
ICC2k = 0.99, $p < 0.01$

Supplemental Figure 8. Functional correlations of FMRI activity between volumes of interest.

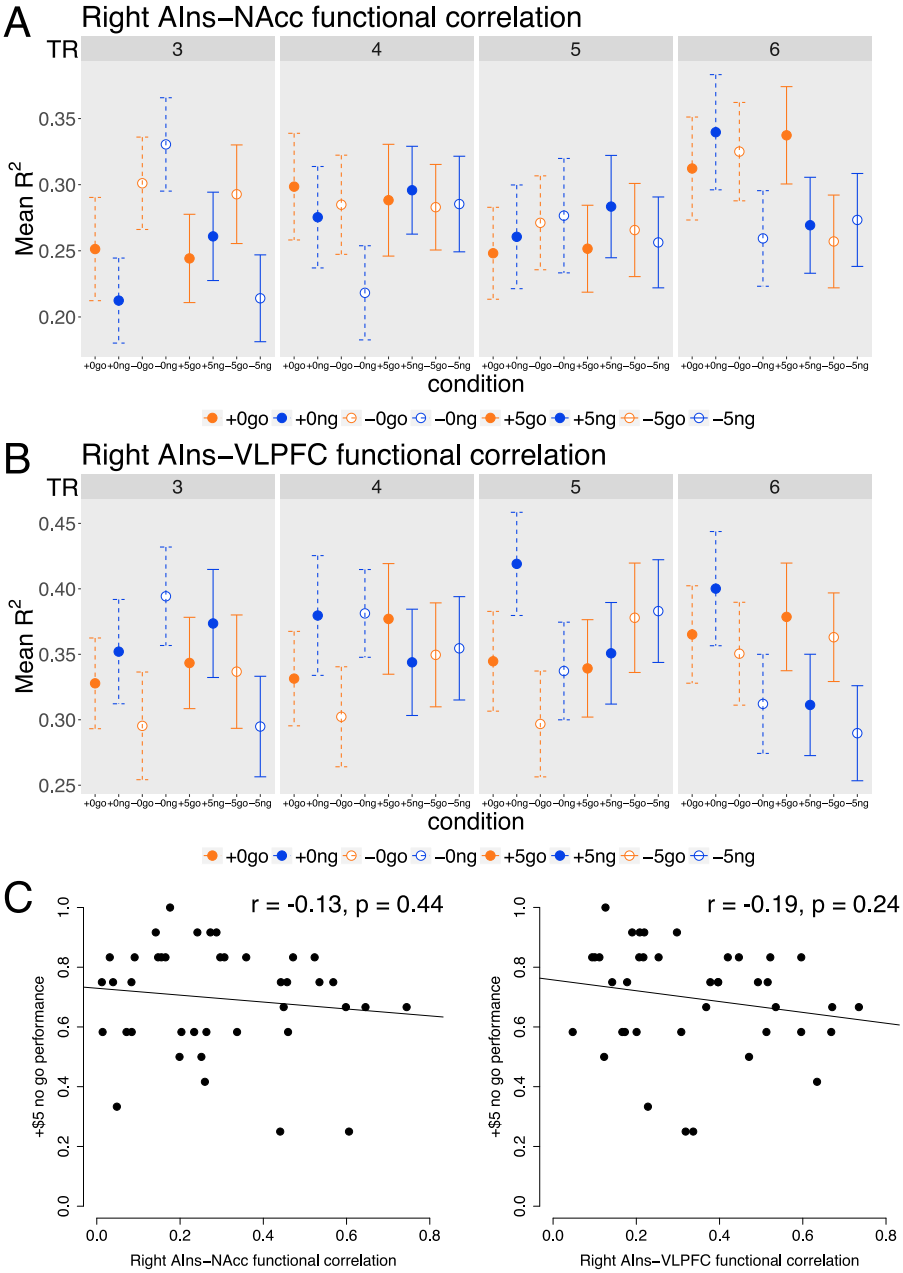

(A, B) Activity time course data was extracted and lagged four seconds (or two TRs) from each VOI (as described in the Materials and Methods). The functional correlation (or "functional connectivity") between VOI pairs (AIns-NAcc and AIns-VLPFC) was assessed by performing simple linear regression between the two VOIs' activity for every trial phase (each linked to a volume acquisition) for each task condition. The variance explained in the regression (R^2) was then averaged across subjects to extract a measure of functional correlation for each trial phase and condition. The plots reveal no significant difference in functional correlation for any particular trial phase or condition.

(C) Right AIns-NAcc functional correlation was not associated with incentivized inhibition behavioral performance (r = –0.13, p = 0.44). Right AIns-VLPFC functional correlation also was not associated with incentivized inhibition behavioral performance (r = –0.19, p = 0.24).

Supplementary Table 1. Associations of right AIns-VLPFC and right AIns-NAcc tract metrics with behavioral performance across all task conditions.
Tract metrics were specifically associated with incentivized inhibition performance (i.e., in +$5 no go trials, predicted associations in **bold**).

Independent Variable: AIns-VLPFC tract inverse mean diffusivity (1–MD)

Dependent Variable: Performance	Coefficient	Std. error	t-statistic	p-value
+$5 go	–0.85	0.87	–0.99	0.33
+$5 no go	**3.61**	**1.38**	**2.62**	**0.01**
+$0 go	0.39	1.21	0.32	0.75
+$0 no go	0.01	1.45	0.01	0.99
-$5 go	1.28	0.80	1.60	0.12
-$5 no go	1.36	1.30	1.05	0.30
-$0 go	–0.53	1.38	–0.39	0.70
-$0 no go	–1.36	1.13	–1.21	0.23

Independent Variable: AIns-NAcc tract fractional anisotropy (FA)

Dependent Variable: Performance	Coefficient	Std. error	t-statistic	p-value
+$5 go	0.27	0.37	0.73	0.47
+$5 no go	**1.46**	**0.59**	**2.48**	**0.02**
+$0 go	–0.13	0.51	–0.25	0.80
+$0 no go	–0.14	0.61	–0.23	0.82
-$5 go	0.15	0.35	0.44	0.66
-$5 no go	0.19	0.55	0.35	0.73
-$0 go	0.03	0.58	0.05	0.96
-$0 no go	–0.30	0.48	–0.63	0.53

Supplementary Table 2.
Associations between right VLPFC activity and behavioral performance during each condition, and between right AIns-VLPFC tract coherence and right VLPFC activity during each condition (predicted associations in **bold**).

Independent Variable: Right VLPFC activity

Dependent Variable: Performance	Coefficient	Std. error	t-statistic	p-value
+$5 go	–0.04	0.07	–0.58	0.57
+$5 no go	**0.38**	**0.13**	**2.84**	**0.01**
+$0 go	–0.19	0.16	–1.21	0.24
+$0 no go	–0.05	0.20	–0.25	0.81
-$5 go	0.03	0.07	0.51	0.62
-$5 no go	–0.11	0.12	–0.90	0.37
-$0 go	–0.03	0.15	–0.18	0.86
-$0 no go	–0.12	0.14	–0.87	0.39

Independent Variable: Right AIns-VLPFC tract inverse mean diffusivity (1–MD)

Dependent Variable: Right VLPFC activity	Coefficient	Std. error	t-statistic	p-value
+$5 go	3.23	1.90	1.70	0.01
+$5 no go	**4.29**	**1.52**	**2.82**	**0.01**
+$0 go	1.14	1.20	0.95	0.35
+$0 no go	1.76	1.15	1.53	0.13
-$5 go	4.87	1.83	2.66	0.01
-$5 no go	1.93	1.69	1.14	0.26
-$0 go	2.07	1.49	1.40	0.17
-$0 no go	–0.16	1.28	–0.13	0.90

Supplementary Table 3. Whole brain FMRI activation peaks.

Contrast: Gain versus Non-gain anticipation					
Region	X	Y	Z	Z-score	Voxels
Right Caudate	10	10	8	13	18163
Left Lingual Gyrus	–10	–92	–15	4.4962	57
Left Middle Temporal Gyrus	–62	–37	–9	4.3712	49
Left Parahippocampal Gyrus	–28	–16	–23	4.503	16
Left Parahippocampal Gyrus	–33	–5	–20	4.0271	13
Right Inferior Temporal Gyrus	45	–16	–18	3.8665	12
Right Parahippocampal Gyrus	25	–22	–20	3.9847	11
Right Superior Temporal Gyrus	48	–25	0	4.0011	10
Right Parahippocampal Gyrus	28	–5	–18	–4.0479	9
Left Middle Frontal Gyrus	–19	30	–15	3.7745	7
Left Medial Frontal Gyrus	–13	21	–18	4.0211	5
Right Inferior Temporal Gyrus	56	–22	–18	3.8012	5
Left Inferior Temporal Gyrus	–57	–31	–20	3.5776	5
Left Parahippocampal Gyrus	–19	–14	–15	–3.7021	5

Contrast: Loss versus Non-loss anticipation					
Region	X	Y	Z	Z-score	Voxels
Left Medial Frontal Gyrus	–13	–2	61	7.3618	19470
Left Postcentral Gyrus	–7	–48	70	3.8751	18
Left Fusiform Gyrus	–22	–92	–15	4.3536	15
Left Cerebellar Tonsil	–36	–54	–44	4.2068	10
Right Superior Temporal Gyrus	54	–37	17	3.7894	9
Right Middle Temporal Gyrus	48	4	–38	3.5988	9
Right Postcentral Gyrus	54	–19	23	3.5848	8
Left Anterior Cingulate	–2	30	3	–4.0953	8
Right Postcentral Gyrus	4	-48	67	3.9553	6
Left Superior Temporal Gyrus	–30	–54	12	3.7236	6
Right Lingual Gyrus	13	–95	–9	4.2643	5
Left Inferior Temporal Gyrus	–39	–5	–35	3.957	5
Left Medial Frontal Gyrus	–4	53	20	–3.7468	5

Contrast: Go versus No go target					
Region	X	Y	Z	Z-score	Voxels

Left Postcentral Gyrus	–51	–25	49	5.9392	601
Right Culmen	16	–46	–20	5.4322	439
Left Medial Frontal Gyrus	–2	–8	55	5.7274	341
Left Supramarginal Gyrus	–54	–57	32	–5.9919	237
Right Inferior Frontal Gyrus	48	4	26	5.3738	175
Left Precentral Gyrus	–57	1	32	5.5156	127
Right Supramarginal Gyrus	48	–54	26	–4.7591	122
Right Putamen	16	7	–3	4.7615	96
Left Thalamus	–16	–22	12	4.8683	79
Left Superior Frontal Gyrus	–7	39	43	–4.665	61
Right Middle Occipital Gyrus	30	–80	–9	–4.7116	60
Left Insula	–39	–5	14	5.3291	58
Right Thalamus	10	–14	8	4.6992	52
Left Caudate	–10	7	3	4.3004	51
Left Cuneus	–16	–89	6	4.6393	47
Right Superior Frontal Gyrus	16	42	40	–4.9683	42
Left Superior Parietal Lobule	–28	–54	46	5.0596	38
Right Cuneus	16	–89	6	5.2612	34
Right Insula	33	15	14	4.109	29
Right Middle Frontal Gyrus	36	15	46	–4.6276	29
Left Middle Frontal Gyrus	–39	7	49	–4.1386	26
Right Inferior Parietal Lobule	33	–48	38	4.0494	22
Right Insula	36	–2	14	5.4581	20
Left Culmen	–13	–48	–15	4.2038	20
Left Inferior Frontal Gyrus	–42	21	6	–4.1167	20
Right Precentral Gyrus	30	–25	52	4.0157	17
Right Postcentral Gyrus	51	–19	32	3.8672	16
Right Middle Frontal Gyrus	33	36	17	4.0639	13
Left Culmen	–22	–60	–23	4.2396	12
Left Putamen	–28	–5	0	3.5043	11
Right Superior Temporal Gyrus	45	10	–23	–4.1415	8
Left Cerebellum	–4	–34	–44	4.3706	6
Left Transverse Temporal Gyrus	–57	–16	12	3.9224	6
Left Precuneus	–13	–46	35	–3.7906	6
Left Middle Frontal Gyrus	–51	15	35	–3.6504	5
Right Inferior Frontal Gyrus	45	27	0	–3.6517	5
Left Superior Frontal Gyrus	–13	12	58	–4.0192	5

Contrast: Gain/Non-gain X Go/No go					
Region	X	Y	Z	Z-score	Voxels
Right Middle Frontal Gyrus	36	7	43	–4.6176	84
Left Middle Frontal Gyrus	–45	21	29	–4.646	67
Left Inferior Parietal Lobule	–48	–48	43	–4.1375	64
Right Angular Gyrus	42	–63	35	–4.3067	32
Left Middle Occipital Gyrus	–22	–89	14	4.4477	21
Right Cuneus	22	–86	12	4.0691	19
Left Precuneus	–36	–72	38	–4.1572	18
Right Middle Occipital Gyrus	36	–72	6	3.6506	7
Right Cingulate Gyrus	16	–16	26	4.1166	6
Left Claustrum	–28	–2	14	3.9788	6
Left Postcentral Gyrus	–48	–19	23	3.9619	5
Right Middle Temporal Gyrus	30	–74	20	3.66	5

Contrast: Loss / Non-loss X Go /No go					
Region	X	Y	Z	Z-score	Voxels
Left Middle Temporal Gyrus	–62	–25	–12	–4.6447	36
Right Cerebellar Nodule	1	–54	–29	3.6883	12
Left Middle Temporal Gyrus	–48	–63	26	–3.6427	6
Right Middle Temporal Gyrus	62	–34	–3	–4.0128	6

Supplementary Table 4. Alternative models with trial-to-trial prediction of incentivized inhibition performance. Logistic regression models that included left hemisphere VOI activity and tract metrics neither improved model fit nor abolished the right hemisphere effects, suggesting the sufficiency of a model including only the right hemisphere. A likelihood-ratio test of nested models was marginally significant ($\chi^2(8) = 15.33$, $p = 0.053$). The logistic regression results presented in Table 2 also reproduced when using NAcc and AIns VOIs defined by the Desai probabilistic atlas. The same model was run with VOI activity that was shifted three volume acquisitions to account for a 6-second hemodynamic lag, but this activity could not predict behavior as in the original model. Since gain incentive cues also increased caudate and anterior cingulate activity (see Figure 2), activity from these VOIs was also included in models, but did not reduce the effects reported in the main text. Interestingly, caudate activity during the target period did predict failure to inhibit motor responses, and VLPFC activity during the target period further predicted successful incentivized inhibition performance in this model.
Z-scores with coefficient estimates and SE in parentheses. *** p < 0.001, ** p < 0.01, * p < 0.05

Variable	Right and left hemisphere	Alternative VOIs (Desai atlas)	Later lag (6 sec)	Caudate and cingulate VOIs
Previous trial go success	1.03 (0.27, 0.26)	1.17 (0.29, 0.25)	0.87 (0.21, 0.24)	1.09 (0.29, 0.36)
Previous trial no go success	–0.55 (–0.17, 0.31)	–0.43 (–0.12, 0.29)	–0.37 (–0.11, 0.29)	0.26 (0.08, 0.31)
R NAcc incentive cue	–2.24* (–4.17, 1.86)	–2.47* (–3.89, 1.58)	–1.56 (–2.32, 1.49)	–2.31* (–4.13, 1.79)
R AIns incentive cue	–0.66 (–1.23, 1.87)	1.61 (2.84, 1.77)	1.11 (1.76, 1.59)	–0.36 (–0.65, 1.81)
R MPFC anticipation	2.67** (1.05, 0.39)	3.68*** (0.80, 0.22)	2.88** (0.46, 0.16)	3.93*** (0.92, 0.23)
R VLPFC target	0.01 (0.004, 0.28)	0.36 (0.08, 0.21)	1.32 (0.29, 0.22)	3.13** (0.84, 0.27)
R DLPFC target	–0.81 (–0.43, 0.53)	–0.21 (–0.08, 0.39)	–1.07 (–0.36, 0.34)	1.27 (0.58, 0.45)
R AIns-NAcc FA	2.43* (9.47, 3.89)	1.72 (5.36, 3.12)	2.01* (5.99, 2.98)	2.18* (7.22, 3.32)
R NAcc*AIns-NAcc FA	2.22* (18.07, 8.14)	2.00* (13.75, 6.87)	1.33 (8.76, 6.59)	2.01* (15.78, 7.86)
R AIns*AIns-NAcc FA	1.11 (9.37, 8.48)	–1.24 (–9.64, 7.79)	–0.66 (–4.67, 7.04)	0.89 (7.26, 8.20)
L NAcc incentive cue	–1.34 (–2.87, 2.14)			
L AIns incentive cue	–0.53 (–1.04, 1.96)			
L MPFC anticipation	–0.55 (–0.21, 0.38)			
L VLPFC target	2.12* (0.58, 0.28)			
L DLPFC target	–0.84 (–0.42, 0.50)			
L AIns-NAcc FA	–1.16 (–4.78, 4.13)			
L NAcc*AIns-NAcc FA	0.82 (7.83, 9.51)			
L AIns*AIns-NAcc FA	0.78 (6.80, 8.73)			
R Caudate target				–5.52*** (–1.97, 0.36)
R Ant. cingulate target				–0.30 (–0.11, 0.35)
Pseudo R^2	0.30	0.22	0.15	0.34
AIC	546	560	576	512
LOOCV %	70.4%	72.1%	72.3%	71.9%

Supplementary Table 5. Trial-to-trial prediction of performance across all conditions. Right AIns and NAcc VOI activity did not predict successful inhibition for incentives other than +$5 (i.e., the incentivized inhibition condition, predicted associations in **bold**). Right MPFC activity, however, predicted successful inhibition for all conditions except for –$0. Right VLPFC activity further predicted failed responses for no gain and no loss incentives, as well as failed inhibition for no loss incentives.

No go target				
Variable	+$5	+$0	–$5	–$0
R NAcc	–**2.02*** (–0.66,	0.69 (0.25, 0.36)	–1.81 (–0.59, 0.32)	–1.24 (–0.53, 0.43)
R AIns	**2.57*** (0.82, 0.32)	–0.93 (–0.31, 0.33)	0.31 (0.09, 0.29)	0.44 (0.19, 0.43)
R MPFC	**3.91***** (0.82, 0.21)	3.02** (0.69, 0.23)	4.04*** (0.78, 0.19)	1.52 (0.40, 0.27)
R VLPFC	0.74 (0.16, 0.22)	1.66 (0.48, 0.29)	–1.75 (–0.41, 0.24)	–2.41* (–0.73,
R DLPFC	–0.57 (–0.22, 0.38)	–0.74 (–0.29, 0.40)	0.21 (0.08, 0.39)	–1.05 (–0.52, 0.49)
Pseudo R^2	0.16	0.19	0.12	0.17
AIC	554	503	584	401
LOOCV %	71.5%	76.3%	70.6%	85.0%

Go target				
Variable	+$5	+$0	–$5	–$0
R NAcc	–1.05 (–0.28, 0.27)	1.81 (0.49, 0.27)	2.09* (0.62, 0.30)	0.93 (0.29, 0.31)
R AIns	–1.07 (–0.30, 0.28)	0.49 (0.13, 0.27)	–1.14 (–0.30, 0.26)	–0.65 (–0.20, 0.31)
R MPFC	–2.07* (–0.38, 0.19)	–0.12 (–0.02, 0.18)	1.20 (0.20, 0.17)	–1.01 (–0.17, 0.17)
R VLPFC	–0.06 (–0.01, 0.19)	–2.25* (–0.49, 0.21)	0.87 (0.17, 0.20)	–2.13* (–0.50,
R DLPFC	0.66 (0.18, 0.28)	–1.05 (–0.36, 0.35)	0.46 (0.14, 0.31)	0.92 (0.33, 0.36)
Pseudo R^2	0.03	0.03	0.02	0.07
AIC	666	649	670	646
LOOCV %	55.6%	55.8%	54.0%	55.8%

Z-scores with coefficient estimates and SE in parentheses. *** $p < 0.001$, ** $p < 0.01$, * $p < 0.05$

Supplementary Table 6. Associations of tract coherence with incentivized inhibition performance after including control variables.
Associations between right AIns-NAcc and right AIns-VLPFC tract coherence and incentivized inhibition performance remained significant or marginally significant after controlling for the coherence of control tracts (preSMA-STN, VLPFC-STN, MPFC-NAcc). Regression results controlling for age, left hemisphere tracts, and both fractional anisotropy (FA) and inverse mean diffusivity (1–MD) are also included, as reported in the main text. Right preSMA-STN 1–MD was not associated with incentivized inhibition performance when tested alone in regression analyses (β = –0.22, t(38) = –1.40, p = 0.17). All coefficient estimates are standardized.

Tract of interest	Control tract	β	t(35)	p-value
Right AIns-NAcc FA		0.39	2.42	**0.02**
	Right preSMA-STN FA	–0.05	–0.28	0.78
	Right VLPFC-STN FA	0.05	0.28	0.78
	Right MPFC-NAcc FA	0.07	0.42	0.68
Right AIns-NAcc FA		0.29	1.88	**0.07**
	Right preSMA-STN 1-MD	0.33	1.86	0.07
	Right VLPFC-STN 1-MD	0.28	1.56	0.13
	Right MPFC-NAcc 1-MD	0.16	0.91	0.37
Right AIns-VLPFC 1–MD		0.42	2.63	**0.01**
	Right preSMA-STN FA	–0.06	–0.32	0.75
	Right VLPFC-STN FA	–0.08	–0.44	0.66
	Right MPFC-NAcc FA	–0.06	–0.36	0.72
Right AIns-VLPFC 1–MD		0.41	2.45	**0.02**
	Right preSMA-STN 1-MD	–0.44	–2.68	0.01
	Right VLPFC-STN 1-MD	0.11	0.57	0.57
	Right MPFC-NAcc 1-MD	0.13	0.81	0.42

Tract of interest	Control variable	β	t(37)	p-value
Right AIns-NAcc FA		0.38	2.49	**0.02**
	Age	–0.001	–0.42	0.68
Right AIns-VLPFC 1–MD		0.39	2.58	**0.01**
	Age	0.01	0.05	0.96
Right AIns-NAcc FA		0.45	2.71	**0.01**
	Left AIns-NAcc FA	–0.18	–1.09	0.28
Right AIns-VLPFC 1–MD		0.42	2.74	**0.01**
	Left AIns-VLPFC 1–MD	–0.13	–0.87	0.39
Right AIns-NAcc FA		0.33	2.23	**0.03**
	Right AIns-NAcc 1–MD	0.28	1.91	0.06
Right AIns-VLPFC 1–MD		0.39	2.58	**0.01**
	Right AIns-VLPFC FA	–0.04	–0.23	0.82

Supplementary Table 7. Predicted and alternative mediation models of the influence of brain structure and function on incentivized inhibition performance.
Alternative mediation models (rows 2-7) verified that only right VLPFC activity statistically mediated the association of right AIns-VLPFC tract coherence with incentivized inhibition. The predicted model (row 1, below) also fit the data better than alternative models (indicated by lower AIC and BIC). An alternative model in which behavioral performance instead mediated the association of structural tract coherence with VLPFC activity was also tested, but the indirect path in this model was only marginally significant, as described in the main text (a*b = 0.12, p = 0.06). A mediation model using this activity reproduced the same pattern of results as the original predicted model, with trending statistical significance. Path coefficients are standardized betas.

Model	a: structure → function	b: function → behavior	c' / c: structure → behavior	Model fit AIC / BIC
R AIns-VLPFC 1–MD → R VLPFC activity → +$5 no go	**0.42** (p < 0.01)**	**0.31* (p = 0.04)**	**c' = 0.26 (p = 0.17) c = 0.39* (p = 0.01)**	**AIC = 329 BIC = 338**
R AIns-VLPFC 1–MD → +$5 no go → R VLPFC activity	0.39* (p = 0.03)	0.30* (p = 0.04)	c' = 0.30 (p = 0.09) c = 0.42* (p < 0.01)	AIC = 329 BIC = 338
R preSMA-STN 1–MD → R VLPFC activity → +$5 no go	0.26 (p = 0.15)	0.51*** (p < 0.001)	c' = -0.35* (p = 0.02) c = -0.22 (p = 0.17)	AIC = 331 BIC = 339
R VLPFC-STN 1–MD → R VLPFC activity → + $5 no go	0.36* (p = 0.03)	0.42** (p = 0.006)	c' = 0.00 (p = 0.99) c = 0.15 (p = 0.35)	AIC = 334 BIC = 343
R AIns-NAcc FA → R VLPFC activity → +$5 no go	0.11 (p = 0.43)	0.38** (p = 0.004)	c' = 0.33* (p = 0.03) c = 0.37* (p = 0.02)	AIC = 334 BIC = 342
R MPFC-NAcc FA → R VLPFC activity → +$5 no go	0.11 (p = 0.40)	0.42** (p = 0.001)	c' = –0.01 (p = 0.94) c = 0.04 (p = 0.81)	AIC = 339 BIC = 348
R AIns-VLPFC 1–MD →R AIns activity → +$5 no go	0.04 (p = 0.80)	0.34* (p = 0.02)	c' = 0.38* (p = 0.02) c = 0.39* (p = 0.01)	AIC = 335 BIC = 343
R AIns-NAcc FA → R NAcc activity → +$5 no go	0.04 (p = 0.82)	0.23 (p = 0.09)	c' = 0.37* (p = 0.03) c = 0.37* (p = 0.02)	AIC = 339 BIC = 347

*** p < 0.001, ** p < 0.01, * p < 0.05